



universität  
wien

# DIPLOMARBEIT

Titel der Diplomarbeit

## Collective Behavior of Water in Carbon Nanotube Membranes

angestrebter akademischer Grad

Magister der Naturwissenschaften (Mag. rer. nat.)

Verfasser:	Georg Menzl
Matrikel-Nummer:	0303529
Studienrichtung:	411 Physik
Betreuer:	Univ.-Prof. Dr. Christoph Dellago

Wien, am 15. Mai 2009



# Danksagung

Ich möchte meinen Eltern für ihre großzügige Unterstützung danken, die mir nicht nur ein sorgenfreies Studium ermöglicht sondern auch in vielen anderen Lebensbereichen geholfen hat.

Besonderer Dank gilt auch den Mitgliedern meiner Arbeitsgruppe, die ein wunderbares Arbeitsklima geschaffen und weit über die Grenzen höflichen Interesses hinaus an meiner Arbeit Anteil genommen haben. Ich kann nur hoffen, dass sich etwas von unseren zahlreichen Diskussionen und ihrem Wissen in der vorliegenden Arbeit widerspiegelt.

Insbesondere danke ich meinem Betreuer Christoph Dellago und Jürgen Köfinger, die mir immer mit kompetentem Rat und anscheinend unerschöpflicher Geduld zur Seite standen. Unsere Zusammenarbeit ist zweifelsohne der krönende Abschluss meiner universitären Ausbildung.

Meine langjährigen Freunde Jaffar und Kalti sind mitverantwortlich dafür, dass ich mein Studium auf vielen Ebenen genießen konnte und unsere Unterhaltungen haben es mir ermöglicht, ein breites Spektrum an Interessen zu wahren.

Zuletzt danke ich der Open Source Gemeinschaft, deren raffinierte und produktivitätssteigernde Hilfsmittel die Arbeit mit Computern erleichtern und bisweilen fast zu einem Vergnügen werden lassen.



## Abstract

We study the properties of a membrane of parallel carbon nanotubes on a quadratic lattice immersed in water. Despite the hydrophobic interior of the nanotubes, the membrane is filled and single-file water chains form due to the positional confinement in the pores. We describe the membrane using a dipole lattice model and perform Monte Carlo simulations to study its phase behavior, observing an order-disorder transition. Analysis of the partition function reveals a relation describing corresponding states of the membrane, which allows us to generalize our model to a wide range of lattice parameters. We investigated the influence of finite size effects on the obtained results to evaluate the significance of our findings for experimentally realizable membranes. The resulting phase diagram shows strong dependence of the critical temperature on the lattice parameters and our data imply that antiferroelectric order does not play a significant role for physical membranes at room temperature.

## Zusammenfassung

Die vorliegende Arbeit behandelt die Eigenschaften einer mit Wasser gefüllten Membran aus parallelen Kohlenstoffnanoröhren auf einem quadratischen Gitter. Trotz der hydrophoben Eigenschaften der Poren werden sie gefüllt und durch die räumliche Einschränkung entstehen eindimensionale Wasserketten. Wir beschreiben die Membran durch ein Dipolgittermodell und studieren ihr Phasenverhalten mit Hilfe von Monte Carlo Simulationen, wobei wir einen Phasenübergang zweiter Ordnung beobachten. Eine Untersuchung der Zustandssumme liefert eine Beschreibung für korrespondierende Zustände der Membran, durch die wir unsere Resultate für unterschiedliche Gitterparameter verallgemeinern können. Die Einflüsse der endlichen Systemgröße in unseren Simulationen auf die erhaltenen Ergebnisse werden untersucht um deren Bedeutung für experimentell realisierbare Membranen abschätzen zu können. Das resultierende Phasendiagramm zeigt starke Abhängigkeit der kritischen Temperatur von den Gitterparametern und unsere Ergebnisse implizieren, dass antiferroelektrische Ordnung bei Raumtemperatur keine signifikante Rolle im Phasenverhalten der Membran spielt.



# Contents

<b>1</b>	<b>Introduction</b>	<b>1</b>
<b>2</b>	<b>Model</b>	<b>3</b>
2.1	Properties of the Membrane . . . . .	3
2.2	The Dipole Lattice Model . . . . .	5
2.2.1	Isolated One-dimensional Water Chains . . . . .	5
2.2.2	Order in Single-file Water Chains . . . . .	6
2.2.3	Defects . . . . .	6
2.2.4	Modelling a Lattice of Single-file Water Chains . . . . .	8
2.3	The Charge Picture . . . . .	9
2.4	Corresponding States of the Membrane . . . . .	12
2.5	Phase Transitions . . . . .	15
2.6	Order Parameter . . . . .	16
<b>3</b>	<b>Methods</b>	<b>21</b>
3.1	Wang-Landau Sampling . . . . .	21
3.2	Biased Sampling . . . . .	24
3.3	Histogram Reweighting . . . . .	26
3.4	Finite Size Effects . . . . .	27
3.4.1	Range of the Interaction Potential . . . . .	27
3.4.2	Multiple Image Convention . . . . .	30
<b>4</b>	<b>Numerical Results</b>	<b>33</b>
4.1	Technical Aspects . . . . .	34
4.2	Domains Revisited . . . . .	35
4.3	Universality Class . . . . .	36
4.4	Influence of System Size on $T_c$ . . . . .	39
4.5	Parametrization of the Multiple Image Convention . . . . .	43
4.6	Corresponding States . . . . .	44

4.7 Phase Diagram . . . . .	47
<b>5 Final Remarks</b>	<b>51</b>

# Chapter 1

## Introduction

Carbon nanotubes attract interest not only for their electrical and mechanical properties but also because they can serve as a nanoscale container for liquids [1]. The interior of carbon nanotubes is hydrophobic, but nonetheless filling-emptying transitions have been observed when a tube is immersed in water [2, 3]. The confinement in narrow single-wall carbon nanotubes leads to the formation of one-dimensional water chains. The properties of these single-file water wires are distinctly different from bulk water in many aspects, such as oriental relaxation, proton transport and solid like ordering [1, 4–6]. In particular, one-dimensional water chains in narrow nonpolar pores exhibit tight nearest neighbour hydrogen bonds which lead to order over large distances [3].

Membranes of carbon nanotubes share structural properties with biological pores which makes them a natural choice for biomimetic systems with a wide range of applications, such as molecular sensing and nanoscale delivery of therapeutics [7]. The possible technical applications of such membranes range from desalination to a significant role in the construction of fuel cells [7–9] and over the last few years the synthesis methods for vertically aligned single-walled carbon nanotubes were refined significantly [10, 11].

Previous studies have shown that the smooth interior of the carbon nanotubes interacts with the water chains in a relatively nonspecific way, confining the water molecules to fixed positions in the tube [3]. The hydrogen bonds between neighbouring water molecules in the one-dimensional chain restrict the dipole moment of the molecules. As a consequence, the interaction between the water molecules in the chain can be described accurately by a dipole lattice model [3, 12, 13]. Using this simple and computationally efficient model, we can reduce the problem to a two-dimensional spin lattice and study its phase behavior. Since the interaction between neighbouring spins favors opposite orientation of their respective dipole

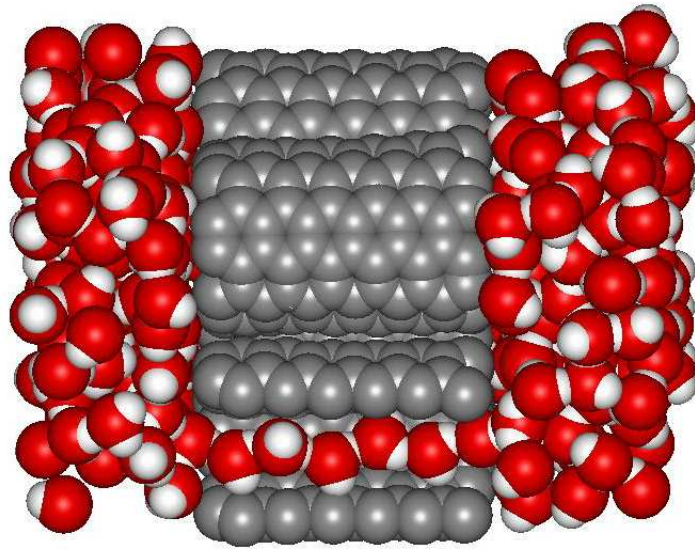


Figure 1.1: Molecular dynamics simulation of a membrane of carbon nanotubes immersed in water. Ordered single-file water chains form within the pores of the membrane [14].

moments, the system is antiferroelectrically ordered for low temperatures. The model shows an order-disorder transition at the critical temperature and we will analyze the effect of different lattice geometries, i.e., tube length and spacing, on the critical point. Due to our investigation of corresponding states on the lattice we can, within the limits of our model, infer the significance of the ordered phase for membranes of experimentally realizable dimensions from our results.

This thesis is structured in the following manner: In Chapter 2 the model used in this work is constructed by incorporation of the properties of narrow carbon nanotubes and one-dimensionally confined water chains. We will introduce a different description for the interaction, the charge picture [3, 12], which will provide insight into the nature of corresponding states on the lattice. In Chapter 3 we will introduce the methods used in simulation. Chapter 4 starts with a study of the influence of finite size effects on the results obtained from simulation before we present the phase diagram of the lattice model. This result is followed by final remarks.

# Chapter 2

## Model

The subject of our study is a membrane consisting of parallel carbon nanotubes on a quadratic lattice. If a membrane of carbon nanotubes with sub-nanometer diameter is immersed in water, the pores of the membrane are filled and due to confinement in the narrow pores the water behaves differently from bulk water, exhibiting properties of great interest such as ordering over large distances. In this work we will focus on the interaction between the water chains in the pores and the resulting phase behavior of the membrane.

In this Chapter, we will describe the model that mimics the water filled nanopores in the membrane and introduce an alternative representation to describe their interaction. Using this representation we are able to derive corresponding states in our model, thus greatly enhancing the implications of the obtained results. Different lattice geometries, i.e., tube lengths  $L$  and lattice constants  $d$ , will be studied to reach conclusions about the effect of these parameters on the phase behavior of the model. After a brief outline of the very basics of the theory of phase transitions, a suitable order parameter for the phase transition of our model is defined.

### 2.1 Properties of the Membrane

The filling and emptying of individual carbon nanotubes with one-dimensional water chains has been studied in molecular dynamics simulations [2]. Using an empirical potential to model the interaction between the water molecules, a filling transition of the hydrophobic carbon nanotubes was observed. The average number of water molecules in the tube is governed by the difference in the local chemical potential between water molecules in bulk and inside the tube. Due to the confinement by the narrow carbon nanotubes, the water molecules in the tube

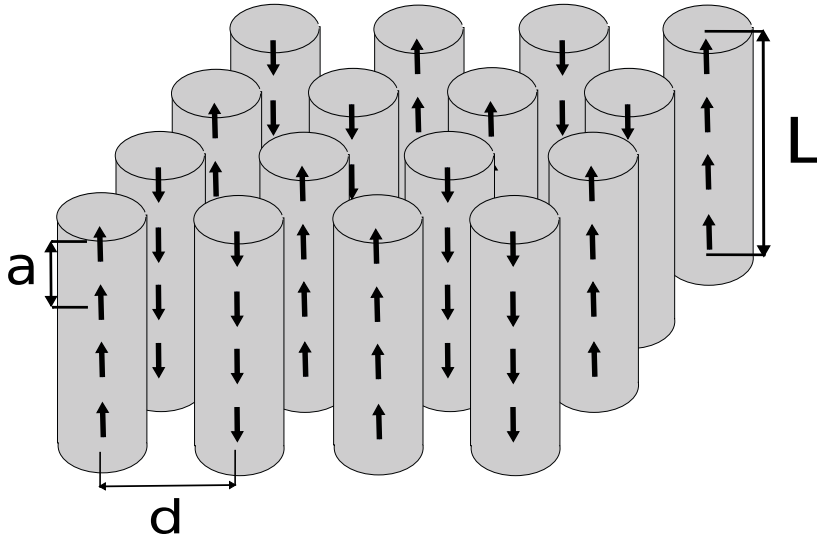


Figure 2.1: Membrane of carbon nanotubes on a quadratic lattice. The water molecules in the pores form single-file water chains due to confinement and the hydrogen bonds between the water molecules.

are aligned in a one-dimensional chain, where the molecules have tight nearest neighbour hydrogen bonds.

Based on these results, we assume that single-file water chains form in the pristine, nonpolar carbon nanotubes of the membrane and that the channels are completely filled during our simulation, which is in good agreement with the results obtained in Ref. [3]. Consequently, we will not include filling-emptying transitions in our model.

The influence of the carbon nanotubes on the interaction between the water molecules were studied in molecular dynamics simulations using empirical potentials [12]. The interaction with the carbon atoms confines the water molecules to a narrow cylindrical volume along the tube axis. Replacing this interaction by soft walls leads to a stronger positional confinement than the interaction with the smooth walls of the carbon nanotubes. However, good agreement with the proton transport properties of the chain has been found in simulation using this interaction [5].

For the sake of simplicity, we assume that the tubes have no effect on the coupling of separate water chains in the membrane (the geometry of the membrane is depicted in Fig. 2.1). Specifically this means that we do not account for screening effects between the water wires. While this premise might seem bold at first sight, it allows us to predict an upper limit for the strength of the coupling between the water chains.

In our simulation we model the interaction of the nanotubes with the water chains by restricting the position of the water molecules to fixed sites along the tube axis with a spacing of  $a = 2.65 \text{ \AA}$  between neighbouring particles, which is the average distance between water molecules in ordered single-file chains obtained from molecular dynamics simulations [3].

We will study the effects of this spatial confinement on the behavior of the water molecules in more detail in the following Section.

## 2.2 The Dipole Lattice Model

In this section we will introduce the dipole lattice model to describe the behavior of single one-dimensional water chains and give an overview of their physical properties. Then we will establish the Hamiltonian for water chains on a quadratic lattice.

### 2.2.1 Isolated One-dimensional Water Chains

The water molecules in a carbon nanotube are represented by a dipole lattice model. It has been shown [3] that the results obtained using this model are in good agreement with the results gained by the implementation of computationally more expensive empirical potentials, such as the TIP3P potential, in describing the properties of single-file water chains in carbon nanotubes.

Due to the strong positional confinement inside a narrow nanotube, the orientation of the hydrogen bonds is nearly aligned with the tube axis [2]. To mimic this confinement, the orientation of the dipoles in our model is restricted to pointing up and down parallel to the tube axis. This reflects the fact that single-file water chains exhibit tight nearest neighbour hydrogen bonds [3].

The dipole moment of the particles in an ordered chain has a fixed direction parallel to the tube axis and a fixed magnitude  $\mu$ , the sign of the vector determines the orientation “up” or “down”:

$$\mathbf{p}_i = \begin{pmatrix} 0 \\ 0 \\ \pm\mu \end{pmatrix}. \quad (2.1)$$

Dipoles representing defects in the chain are orthogonal to this dipole moment (see Subsection 2.2.3). The dipole-dipole interaction between dipoles in a single-file chain is given by

$$\Psi(\mathbf{r}_{ij}, \mathbf{p}_i, \mathbf{p}_j) = -\frac{3(\mathbf{r}_{ij} \cdot \mathbf{p}_i)(\mathbf{r}_{ij} \cdot \mathbf{p}_j) - r_{ij}^2 \mathbf{p}_i \cdot \mathbf{p}_j}{r_{ij}^5} \quad (2.2)$$

in Gaussian units, where  $\mathbf{r}_{ij}$  is the distance vector between the two point dipoles and  $\mathbf{p}_i$  and  $\mathbf{p}_j$  are their respective dipole moments.

This approximation does not account for the rotational freedom of the molecules around the tube axis. The OH bond which does not participate in the hydrogen bonding with the next molecule in the chain is able to rotate without disrupting the hydrogen bonds with the particle's neighbours, which results in increased rotational freedom in comparison to bulk water [4]. However, the impact of these rotations on the interaction between the molecules is small and is therefore neglected in our model.

### 2.2.2 Order in Single-file Water Chains

The dipole-dipole interaction potential (2.2) implies that dipoles with identical orientation within a chain are energetically favored. We will refer to a configuration where all dipoles in a chain have identical orientations as the “ordered” state of the chain.

We know from statistical mechanics that such one-dimensional dipole chains do not exhibit an order-disorder phase transition, as the potential for such a transition to occur in one dimension at  $T > 0$  has to decay slower than [15]

$$\Psi_{ij}(\mathbf{r}) \propto \frac{1}{r^2}. \quad (2.3)$$

This implies that in the limit  $N \rightarrow \infty$  long range order is destroyed by thermal fluctuations.

Although there is no phase transition in the thermodynamic limit, one-dimensional water chains exhibit ordering of the dipole moment of the particles over large distances. Water wires in confinement show ordering up to a distance of approximately 0.1 mm at room temperature [3]. This order is crucial for the proton transport properties of water-filled carbon nanotubes and it is of great interest in a wide range of fields, such as biology and engineering [9, 16].

### 2.2.3 Defects

The thermal excitations that destroy the long-range order in the dipole chain are hydrogen bonding defects.

In the ordered state of a chain all dipoles point in the same direction. This state in our model represents an arrangement in which each molecule forms OH bonds with its nearest neighbours, donating one hydrogen bond and accepting one. If we have a defect in our chain this is no longer the case.

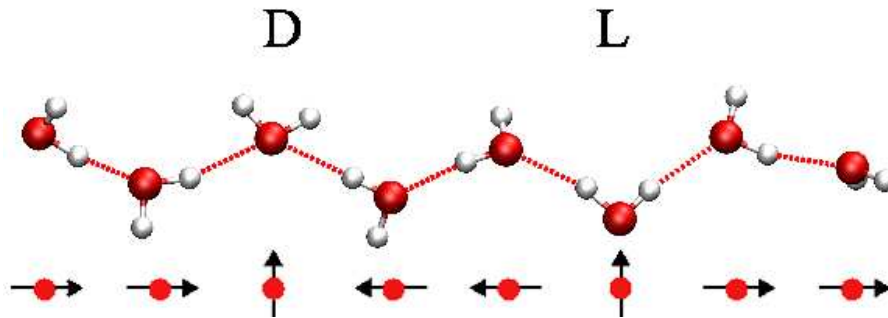


Figure 2.2: Schematic representation of defect configurations in a one-dimensional water chain in a molecule representation (top) and in the dipole picture (bottom). In case of the D-defect the defect molecule accepts two hydrogen bonds, in an L-defect configuration it donates two hydrogen bonds. In the dipole picture both defects are represented by dipoles pointing in a direction orthogonal to the tube axis [3].

There are two possible configurations with atypical hydrogen bonding which we consider a defect: a molecule can either donate two hydrogen bonds and accept none or it donates none and accepts two hydrogen bonds. In reference to defects in hexagonal ice, the former is called L-defect and the latter D-defect (see Fig. 2.2). In both cases the dipole moment of the water molecule is on average orthogonal to the tube axis. Thus, a defect is represented by a point dipole orthogonal to the tube axis in the dipole picture. A defect in the chain connects two ordered chain segments with opposite orientations.

The energetics of such defects are one of the key properties affecting the behavior of water wires in carbon nanotubes [13]. However, in this work we aim to study a basic model for the membrane and we will avoid the numerical challenges associated with the inclusion of defects in our model. Furthermore, isolated tubes exhibit order over large distances at room temperature and preliminary results indicate that the arrangement of tubes on a quadratic lattice increases this effect, thus justifying the omission of defect formation in our model.

This simplification facilitates the determination of an upper bound for the critical temperature in membranes with a given geometry. The ordered state of the membrane, i.e., the configuration with the lowest free energy, consists of defect free chains in a specific pattern. By the exclusion of defect formation from our model, the temperature for which a membrane with given length and spacing of the tubes exhibits order is equal to or higher than the temperature one would

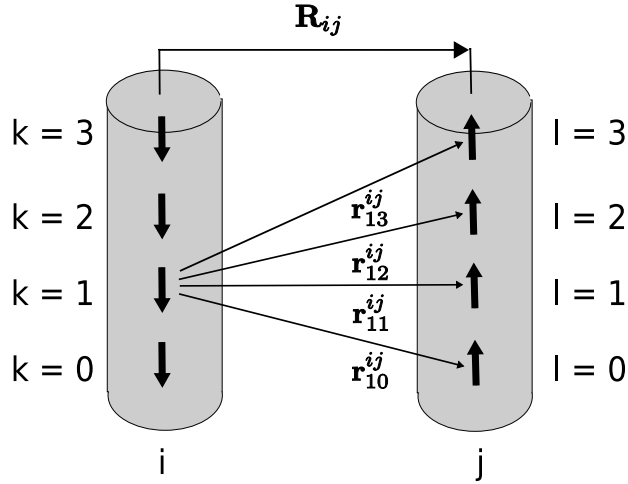


Figure 2.3: Interaction between two chains on the lattice in the dipole picture. The interaction energies between chain  $i$  and  $j$  is obtained by summing the dipole-dipole interactions between the chains over  $k$  and  $l$ . To facilitate visualization the interaction between the dipole at position  $k = 1$  in tube  $i$  with all dipoles in tube  $j$  is depicted. The distance vector between two dipoles belonging to different chains  $\mathbf{r}_{kl}^{ij}$  is given by the sum of the distance vector between the chains in the  $xy$ -plane  $\mathbf{R}_{ij}$  and the vertical distance vector  $a(l - k)\mathbf{e}_z$ .

obtain in a model that allows for defects.

#### 2.2.4 Modelling a Lattice of Single-file Water Chains

Since the dipole lattice model mimics the behavior of single one-dimensional water chains well, we are confident that this model is also suitable to describe the interaction between the parallel water chains found in a membrane.

As we do not allow for defect formation in the dipole chains, all dipoles in a chain have identical orientation. We will utilize this property when establishing the Hamiltonian for the lattice of dipole chains by summing the interaction between two chains on the lattice over the individual chains. The resulting interaction  $\Phi(\mathbf{R}_{ij})$  between two tubes  $i$  and  $j$  aligned orthogonally to the  $xy$ -plane, depicted in Fig. 2.3, is given by

$$\begin{aligned} \Phi(\mathbf{R}_{ij}) &= \sum_{(k,l)} \Psi(\mathbf{r}_{kl}^{ij}, \mathbf{p}_k, \mathbf{p}_l) \\ &= \sum_{(k,l)} -\frac{3(\mathbf{r}_{kl}^{ij} \cdot \mathbf{p}_k)(\mathbf{r}_{kl}^{ij} \cdot \mathbf{p}_l) - (r_{kl}^{ij})^2 \mathbf{p}_k \cdot \mathbf{p}_l}{(r_{kl}^{ij})^5}, \end{aligned} \quad (2.4)$$

where the dipole-dipole interaction is summed over all particles in the tubes  $i$

and  $j$  and  $\mathbf{r}_{kl}^{ij}$  is defined as

$$\mathbf{r}_{kl}^{ij} = \mathbf{r}_l^j - \mathbf{r}_k^i, \quad (2.5)$$

where

$$\begin{aligned} \mathbf{r}_k^i &= \mathbf{R}_i + ak \mathbf{e}_z \\ \mathbf{r}_l^j &= \mathbf{R}_j + al \mathbf{e}_z, \end{aligned} \quad (2.6)$$

where  $a$  is the dipole-dipole spacing in the individual tubes. This leads to

$$\begin{aligned} \mathbf{r}_{kl}^{ij} &= \mathbf{R}_j + al \mathbf{e}_z - \mathbf{R}_i - ak \mathbf{e}_z \\ &= \mathbf{R}_{ij} + a(l - k) \mathbf{e}_z. \end{aligned} \quad (2.7)$$

Summing over the interactions of the tubes reduces the model to a two-dimensional spin lattice with Hamiltonian

$$\begin{aligned} H(\{s(\mathbf{r})\}) &= \sum_{(i,j)} s_i s_j \Phi(s_i, s_j, \mathbf{R}_i, \mathbf{R}_j) \\ &= \sum_{(i,j)} s_i s_j \Phi_{ij} \end{aligned} \quad (2.8)$$

where  $s_i$  and  $s_j$  give the orientation of the tubes  $i$  and  $j$  containing  $L$  particles each

$$s_i = \frac{1}{\mu L} \sum_l^L \mathbf{p}_l \cdot \mathbf{e}_z \quad (2.9)$$

which restricts the possible values for  $s_i$  and  $s_j$  to 1 or  $-1$ , respectively. The sum is evaluated over all tube pairs on the lattice

$$\sum_{(i,j)} := \frac{1}{2} \sum_i \sum_j \quad \text{where } i \neq j. \quad (2.10)$$

In accordance with conventions in statistical mechanics we will subsequently refer to the single-file water chains on the two-dimensional lattice as “spins”.

### 2.3 The Charge Picture

The charge picture is an alternative way to describe the energetics of one-dimensionally confined water chains. While it was originally devised to describe the behavior of excess charges in a single confined water chain [5], the charge picture will soon prove to be useful in describing the interaction of ordered chains with each other. Its main advantages are a better insight in the nature of the interactions as well as reducing the computational cost, thus making large systems computationally accessible [3].

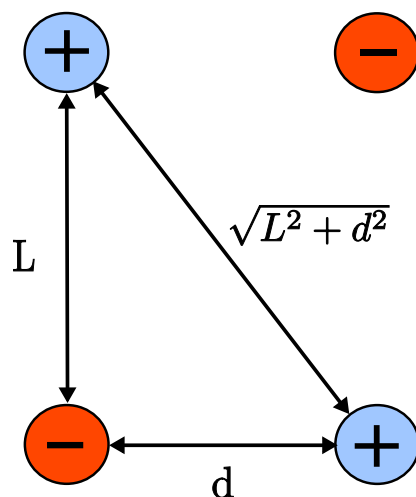


Figure 2.4: Two chains of opposite orientation in the charge picture. The interaction between the two tubes is given by the interaction of the Coulomb charges at the chain ends.

Investigating the properties of proton transport through water filled carbon nanotubes via molecular dynamics simulations, the interaction between an excess charge and the end points of the water chain was calculated [5]. This interaction was found to have Coulomb-like properties and the model was subsequently used and refined to describe the formation and movement of defects in water chains in the interior of carbon nanotubes [3].

Since we do not aim to describe the energetics of defects within the tube, it seems promising to investigate how well the model of two Coulomb charges at the end points of the tubes describes the interaction between multiple tubes in the membrane. We will focus on the fact that the charge picture gives us the opportunity to describe the interaction between the chains on the lattice in simple terms, thus leading to a model for the corresponding states of the system.

The advantage of treating the system in the charge picture is obvious: Instead of summing over all dipoles located in the tube, we can simply calculate the interaction energy between the two charges sitting at the end of each tube (see Fig. 2.4). Regardless of the number of molecules in the water chain, the calculation of the interaction between two chains is reduced to the interaction between two pairs of Coulomb point charges.

In the charge picture, the interaction between two parallel water chains at a

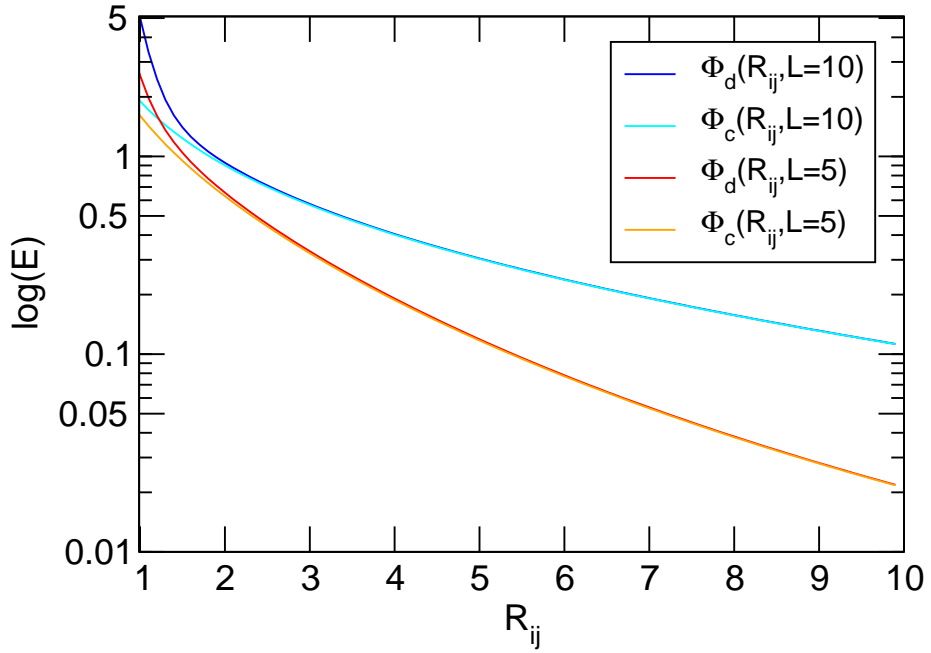


Figure 2.5: Comparison between the interaction energy  $E$  of two tubes at a distance  $R_{ij}$  in the charge picture and in the dipole picture. Except for very small distances, the interaction energies computed in the charge picture agree excellently with those obtained from the dipole-dipole interaction. Energy and length are given in reduced units.

distance  $\mathbf{R}_{ij}$  from each other can be expressed as

$$\Phi(\mathbf{R}_{ij}, L) = s_i s_j 2 \left[ \frac{1}{R_{ij}} - \frac{1}{\sqrt{R_{ij}^2 + L^2}} \right] \quad (2.11)$$

where  $L$  is the length of the water chain and  $R_{ij} = |\mathbf{R}_{ij}|$ . Inserting this interaction potential in Eq. (2.8) yields the Hamiltonian for the system in the charge picture.

The charge picture describes the energetics of an isolated single-file water chain in an exact manner, interpreting the interaction as Coulomb-like. This Coulomb-like behavior can be approximated with excellent accuracy by Coulomb interactions. Fig. 2.5 provides an insight into the numerical accuracy of this approximation for chain-chain interaction. For the investigated chain lengths  $L = 5$  and  $L = 10$  the agreement with the calculation in the dipole picture from Eq. (2.4) is remarkably good except for very small tube spacings.

For short distances the interaction in the charge picture is dominated by the interaction of the neighbouring Coulomb charges. As shown in Fig. 2.6, for larger distances between the tubes the contribution of the charges at a distance

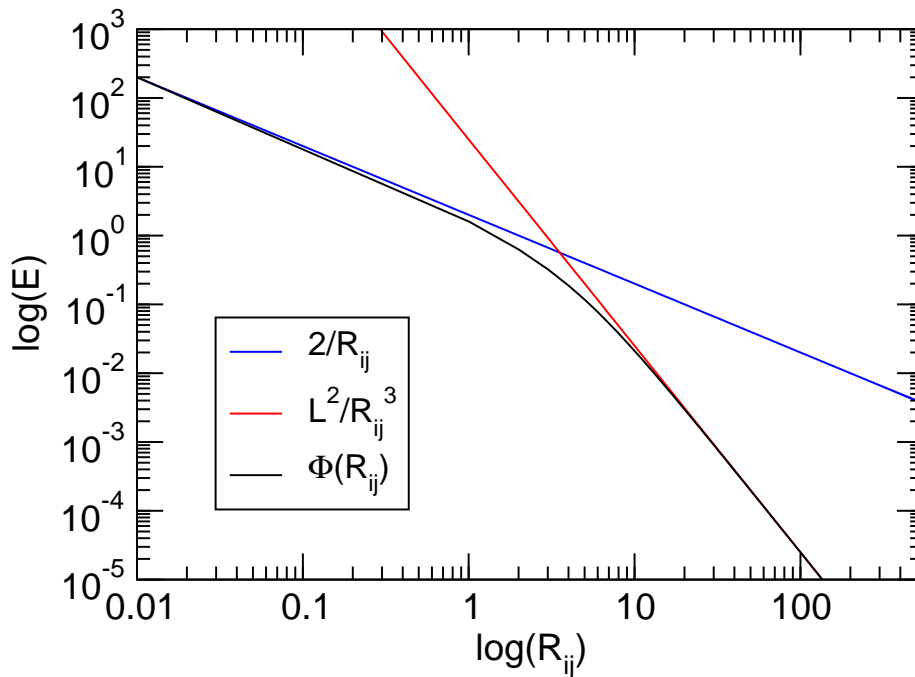


Figure 2.6: Interaction energy  $E$  of two chains with identical orientation with length  $L = 5$  at as a function of distance  $R_{ij}$  in the charge picture. For very short distances the interaction resembles Coulomb charge interaction (blue line), for large distances it changes to dipole-dipole interaction (red line). Energy and length are given in reduced units.

$\sqrt{L^2 + R_{ij}^2}$  becomes more important and the interaction resembles the interaction of two dipoles with length  $L$ .

Our analysis suggests that the interaction between parallel dipole chains can be approximated by the charge picture with good accuracy.

## 2.4 Corresponding States of the Membrane

In this section we will describe the interactions between the single-file water chains in the membrane pores in the charge picture. Using this approach we can formally derive the behavior of the interaction energy in our model as a function of the tube length  $L$  and tube spacing  $d$ . This will allow us to apply our simulation results to a wide range of lattice configurations and, in particular, it will give us the opportunity to relate these results to membranes of a scale realized in experimental work [7, 17].

Since the tubes are located on the sites of a quadratic lattice, we can express the orthogonal distance between two tubes  $i$  and  $j$  on the lattice  $\mathbf{R}_{ij}$  as multiples

of the tube spacing  $d$

$$\mathbf{R}_{ij} = d \begin{pmatrix} m \\ n \\ 0 \end{pmatrix}, \quad (2.12)$$

where  $m$  and  $n$  are integers. The translation invariance of the potential implies that its value only depends on the absolute value of the distance vector  $\mathbf{R}_{ij}$

$$R_{ij} = \sqrt{m^2 + n^2} d. \quad (2.13)$$

This allows us to write Eq. (2.11), the interaction energy between two spins  $s_i$  and  $s_j$  in the charge picture, in the form

$$\Phi(R_{ij}, L) = s_i s_j 2 \left[ \frac{1}{\sqrt{m^2 + n^2} d} - \frac{1}{\sqrt{(m^2 + n^2) d^2 + L^2}} \right] \quad (2.14)$$

or

$$\Phi(R_{ij}, L) = s_i s_j \frac{2}{d} \left[ \frac{1}{\sqrt{m^2 + n^2}} - \frac{1}{\sqrt{(m^2 + n^2) + \left(\frac{L}{d}\right)^2}} \right]. \quad (2.15)$$

Therefore, if the ratio between  $L$  and  $d$  is constant, the interaction energy between two tubes is inversely proportional to  $d$ . If

$$\frac{L}{d} = \frac{L'}{d'} \quad (2.16)$$

holds for two different membranes, the relationship between the two interaction potentials  $\Phi$  and  $\Phi'$  on the respective lattices is given by

$$d\Phi = d'\Phi'. \quad (2.17)$$

Alternatively, one could keep the spacing between the tubes constant and vary the length of the tubes. For a constant ratio between  $L$  and  $d$  the interaction is given by

$$\Phi(R_{ij}, L) = s_i s_j \frac{2L}{Ld} \left[ \frac{1}{\sqrt{m^2 + n^2}} - \frac{1}{\sqrt{(m^2 + n^2) + \left(\frac{L}{d}\right)^2}} \right] \quad (2.18)$$

hence

$$L\Phi = L'\Phi'. \quad (2.19)$$

So far we have shown that the dependence of the interaction potential on different system sizes is mathematically very convenient to handle in the charge picture. The interaction energy  $\Phi_{ij}$  between parallel water chains for a given ratio between the length of the tubes and the distance between the tubes is

inversely proportional to the length of the tube. If one attempts to simulate large systems, it is therefore easily possible to calculate the interaction energies with low computational cost.

However, a closer look at the canonical partition function reveals the true relevance of the derived properties. The canonical partition function is given by

$$\begin{aligned} Z(\beta, L) &= \sum_{\Gamma} \exp \left[ -\beta \sum_{(m,n)} \Phi(d, L) \right] \\ Z(\beta, L) &= \sum_{\Gamma} \exp \left[ -\frac{\beta}{L} \sum_{(m,n)} L\Phi(d, L) \right] \end{aligned} \quad (2.20)$$

where  $\sum_{\Gamma}$  is the sum over all points in configuration space and  $\sum_{(m,n)}$  is the sum over all spin pairs on the lattice according to Eq. (2.10).

If Eq. (2.16) holds, this leads to

$$Z(\beta, L') = \sum_{\Gamma} \exp \left[ -\frac{\beta}{L'} \sum_{(m,n)} L'\Phi(d', L') \right] \quad (2.21)$$

and defining

$$\beta' = \frac{L'}{L} \beta \quad (2.22)$$

we obtain

$$Z(\beta', L') = Z(\beta, L) . \quad (2.23)$$

If one calculates the distribution function of the order parameter for a system at a given temperature, we can immediately derive an inverse temperature  $\beta'$  for which the distribution function is identical, for any system that obeys Eq. (2.16).

In terms of the temperature  $T$  Eq. (2.22) yields

$$T' = \frac{L}{L'} T \quad (2.24)$$

which is by Eq. (2.17) equivalent to

$$T' = \frac{d}{d'} T . \quad (2.25)$$

Therefore, a membrane composed of short tubes at a temperature  $T$  will behave identically to a membrane of longer tubes at a lower temperature  $T'$ , provided that Eq. (2.16) is satisfied.

As we will focus our investigations on the phase transition of the system, this property is of special interest for the critical temperature  $T_c$ . If  $T_c$  for one system with a given ratio between tube length and tube spacing is known, the critical temperature for all other systems with that same ratio can be easily calculated.

In a similar manner our model can be adopted to incorporate a dielectric constant  $\epsilon_r$  to account for screening effects caused by the interaction with the nanopore walls. Analogous to Eq. (2.20), the temperature of the corresponding state is given by  $\tilde{T} = \epsilon_r T$ .

## 2.5 Phase Transitions

The phase behavior of lattice spin systems has been subject to extensive research [18,19]. Arguably the most famous example for a lattice model exhibiting a phase transition is the two-dimensional Ising model, which shows an order-disorder transition at the critical temperature  $T_c$  in the absence of an external field  $H$ . The analytical solution for this model was obtained by Onsager [20] and renewed the research interests of physicists in the Ising model and similar models, which are considerable simplifications of physical systems. The possibility of studying complex phenomena like phase transitions in a comparatively simple system improves the understanding of the underlying principles and therefore leads to improved models for more complex systems.

A phase transition of second order on a spin lattice is characterized by the spontaneous breaking of the system's symmetry. As opposed to a phase transition of first order, the first derivatives of the free energy show analytic behavior at the critical temperature  $T_c$ . The Helmholtz free energy is given by

$$F_N(\beta, V) = -\frac{1}{\beta} \ln Z_N, \quad (2.26)$$

where  $Z_N$  is the canonical partition function

$$Z_N = \sum_{\nu} \exp(-\beta E_{\nu}), \quad (2.27)$$

where the sum is taken over all states  $\nu$ . The derivative of the free energy per particle

$$f(\beta, h) = \frac{F(\beta, h, N)}{N} \quad (2.28)$$

with respect to the dimensionless external field  $h$

$$h = \beta H \quad (2.29)$$

is the response function of the system to changes in the external field

$$\eta(T, h) = -\frac{\partial f}{\partial h}. \quad (2.30)$$

The 2D Ising model shows a nontrivial phase transition of second order in the absence of an external field and an additional parameter is needed to describe

the phase behavior of the system [18]. This additional parameter is the order parameter.

## 2.6 Order Parameter

Before we specify the order parameter for our system, we will precede with the general properties we demand from our order parameter  $\eta$ :

$$\begin{aligned} \eta &= 0 & \text{for } T > T_c \\ |\eta| &> 0 & \text{for } T < T_c \end{aligned} \tag{2.31}$$

Obviously, these mathematical properties are not sufficient to define an order parameter which describes the degree of order in a system in a reasonable way. The choice of the order parameter is motivated by the behavior of the system and depends to a large extent on the intuition of the scientist trying to faithfully describe the spontaneous breaking of symmetry which characterizes an order-disorder transition [21].

Interpreting the membrane as a spin lattice, each single-file water chain is represented by a spin which can either point “up” or “down”. As the interaction between the spins renders configurations with spins of the same value next to each other unfavorable, we expect the ground state in our model to resemble the ground state in the antiferromagnetic two-dimensional Ising model<sup>1</sup>. The ground state we observe in simulation is indeed equivalent to the ground state of the antiferromagnetic two-dimensional Ising model, shown in Fig. 2.7: Neighbouring spins on the lattice have opposite orientation. Thus we choose to implement the order parameter  $\eta$  which is known from antiferroelectric and antiferromagnetic systems: the staggered magnetization.

To calculate  $\eta$ , the lattice is divided into sub-lattices defined in the following manner: Each lattice point belongs to one of the two sub-lattices and its four nearest neighbours belong to the other sub-lattice. Each spin on the quadratic lattice has a unique position which is described by the variable  $i$  in x-direction and  $j$  in y-direction, respectively.

To obtain the staggered magnetization  $\eta$ , the sums over the two sub-lattices are calculated and subtracted from another. Each of the two sub-lattices  $A$  and  $B$  has a ferroelectric order parameter and the subtraction of those sub-lattices

---

<sup>1</sup>For a more detailed study of the behavior of our model in comparison to the two-dimensional Ising model, please refer to Sec. 4.3.

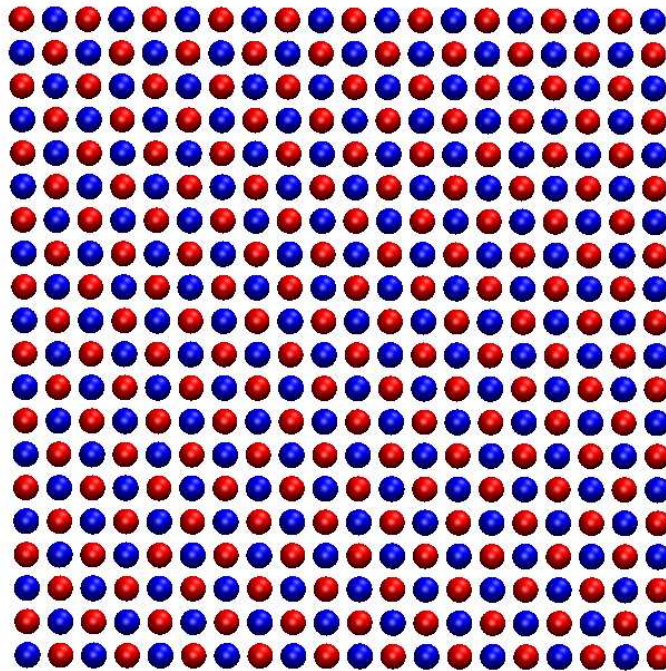


Figure 2.7: Top view on a membrane consisting of 400 tubes in the energetic ground state. The spins on the two sub-lattices  $A$  and  $B$  are oriented in opposite directions. Spins pointing “up” are represented by blues spheres, spins pointing “down” by red spheres. Visualizations of lattice spin systems in this Section were made using the VMD software package [22].

creates our antiferroelectric order parameter

$$\eta = \frac{1}{N} \left[ \sum_{(i,j) \in A}^{I,J} s_{ij} - \sum_{(i,j) \in B}^{I,J} s_{ij} \right] \quad (2.32)$$

with the total number of spins

$$N = IJ \quad (2.33)$$

and  $\sum_{(i,j)}$  defined analogously to Eq. (2.10).

Consequently, a system configuration where the spins on each of the sub-lattices have identical orientations, but the sub-lattices are oriented in opposite directions, maximizes  $|\eta|$ . In this energetically most favored state any two neighbouring spins have values of opposite sign. For low temperatures  $T \ll T_c$  the system is predominately in this ground state, thus yielding a high value of  $|\eta|$ . For higher temperatures, less ordered, i.e., energetically more expensive, states which are entropically more favorable become more and more likely thus decreasing the value of  $|\eta|$ .

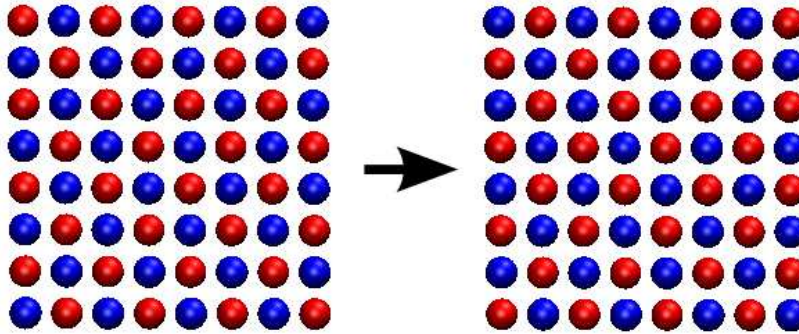


Figure 2.8: Flipping every spin of the left configuration  $a$  creates an energetically equivalent configuration  $b$  with staggered magnetization  $\eta_b = -\eta_a$ . This is true for any given configuration of spins on the lattice.

Since the interaction energy between two spins at a distance  $r$  on the lattice only depends on their orientation relative to each other (see Eq. (2.8)), the system is symmetric with respect to a flip of all spins on the lattice. Each state has an equivalent state of identical energy and reversed polarization which can be reached by said spin flip operation. Due to the symmetry of our spin system towards this operation, known as  $\mathbb{Z}_2$  symmetry, we cannot use the canonical mean value of  $\eta$  as order parameter which we will illustrate by a little gedankenexperiment.

Let us imagine a system where for one half of the simulation run the system is in state  $a$  and the other half of the runtime in state  $b$  as shown in Fig. 2.8. The two states in Fig. 2.8 are energetically equivalent to each other but the mean value of  $\eta$  after the simulation run equals zero, although the configuration of the system is actually perfectly ordered in one of its two energetic ground states at all times.

This is rarely a problem in the theoretical treatment of phase transitions as the mathematically precise definition of the order parameter is given by [23]

$$\eta = \lim_{h \rightarrow 0^+} \lim_{N \rightarrow \infty} \frac{1}{N} \left\langle \sum_{(i,j) \in A}^{I,J} s_{ij} \right\rangle - \lim_{h \rightarrow 0^-} \lim_{N \rightarrow \infty} \left\langle \sum_{(i,j) \in B}^{I,J} s_{ij} \right\rangle. \quad (2.34)$$

When an external field is applied, the  $\mathbb{Z}_2$  symmetry of the system is destroyed by the interaction of the spins with the external field. In the limit  $N \rightarrow \infty$  for  $T < T_c$  spontaneous breaking of the symmetry occurs and letting the fields amplitude decay to zero causes one type of state, the states where a majority of the spins on a sub-lattice is pointing in the direction favored by the interaction with the

external field, to be more favorable than the other. Therefore, the canonical mean of the staggered magnetization  $\langle \eta \rangle$  will be nonvanishing for  $T < T_c$ . It should be noted that the limits  $N \rightarrow \infty$  and  $h \rightarrow 0$  do not commute in this case. In fact,

$$\lim_{N \rightarrow \infty} \lim_{h \rightarrow 0^+} \frac{1}{N} \left\langle \sum_{(i,j) \in A}^{I,J} s_{ij} \right\rangle - \lim_{N \rightarrow \infty} \lim_{h \rightarrow 0^-} \left\langle \sum_{(i,j) \in B}^{I,J} s_{ij} \right\rangle = 0. \quad (2.35)$$

This mathematical “trick” of breaking the symmetry is not necessary in physical systems<sup>2</sup> as for systems of sufficient size spontaneous breaking of the symmetry occurs and the system arbitrarily adopts one of the two degenerate ground states. For  $T < T_c$  the large free energy barrier separating the degenerate ground states prohibits switches between those two states.

In our simulations we cannot reach the thermodynamic limit as this would require an infinitely large system. Clearly, we will need to find a different function from the canonical mean of the order parameter  $\langle \eta \rangle$  to describe the degree of order in our system.

One might suggest the canonical average of the absolute value of the staggered magnetization  $\langle |\eta| \rangle$  instead of  $\langle \eta \rangle$  as an order parameter because it will yield the desired value in the case described above, where the system switches between two states with a high value for  $|\eta|$  at low temperatures. This choice immediately leads to problems at temperatures  $T > T_c$ . At these temperatures the mean value of a well chosen order parameter should be zero according to definition (2.31).

However, if the system is of finite size, which is a limitation hard to overcome in computational simulations, we have to deal with fluctuations in the order parameter of the system not only in the vicinity of the critical point but for all temperatures. These fluctuations cannot cancel if  $\langle |\eta| \rangle$  is used as the order parameter and therefore its value will not vanish for  $T > T_c$ .

To solve this problem, we will compute the distribution function of the staggered magnetization  $\eta$ :

$$p(\eta) = \sum_{\nu} \frac{\exp[-\beta H_{\nu}] \eta_{\nu} \delta_{\eta \nu}}{Z}. \quad (2.36)$$

We can obtain the value of  $\eta$  from the distribution by neglecting one arm of the curve due to symmetry and taking the mean value of the resulting curve. By implementing this method it is possible to study the behavior of  $\eta$  for various temperatures and thus to obtain a phase diagram of the system.

---

<sup>2</sup>Actually, for antiferroelectric systems such an external field cannot even be realized in experiment [18].

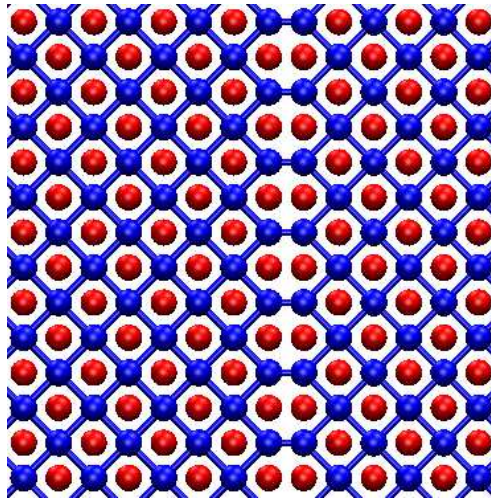


Figure 2.9: A domain wall separating two perfectly ordered domains which are shifted against each other. The spins pointing “up” were connected to each other in the representation to make it easier to identify the domain walls.

The distribution function of the order parameter, and therefore the values for  $\eta$  obtained by the procedure described above, is subject to finite size effects [24] due to the strongly increased correlation length of observables in the vicinity of the critical temperature which cannot be modelled accurately in a finite simulation box. Attempting to correct the obtained data from these finite size effects can lead to cumbersome and computationally expensive procedures. We choose the basic method of comparing the distribution function of the order parameter with the appropriate universal distribution function at the critical point. This approach will be described in detail in Sec. 4.3.

However, one type of configurations cannot be detected by the order parameter we implemented, namely, configurations with phase separation. These configurations are associated with the formation of domains, i.e., parts of the lattice are in the anti-ferroelectrically ordered state but shifted against each other so that their contributions to  $\eta$  cancel each other. Where those ordered parts meet on the lattice, a domain wall is formed. Domain walls do not cross each other, consequently they form closed curves on the lattice [18]. One particularly stable configuration is formed by domain walls which run from one boundary of the lattice to the other as shown in Fig. 2.9. It should be kept in mind, however, that with the use of periodic boundary conditions those domain walls also take on the shape of closed curves.

The occurrence of phase separation involving domains of ordered states will be treated in more detail in Chapter 4.

# Chapter 3

## Methods

Monte Carlo simulation techniques are the natural choice for simulating systems which have no natural dynamics [25]. This is clearly the case for our model with its discrete degrees of freedom for the orientation of the chains' dipole moments. Although this approximation describes the properties of one-dimensional water chains sufficiently, it is important to note that the introduced restriction in orientation destroys any natural dynamic in the system.

During our investigation of the model system we encountered challenges with respect to the quality of the sampling of configurations in the system. Due to the high barriers in the free energy landscape, the configuration space cannot be sampled efficiently by use of the Metropolis Monte Carlo technique [26]. Also, when we want to determine the critical point of our model, we aim to avoid performing large numbers of simulations in a small temperature range in the vicinity of  $T_c$ . The first three sections are devoted to the detailed description of these problems and the methods we implemented to manage them. The influence of finite size effects on our simulation results is investigated in the second part of the Chapter.

### 3.1 Wang-Landau Sampling

The aforementioned formation of domains causes difficulties in our attempt to describe the state of the system by the chosen order parameter. In a system with two domains (see Fig. 2.9) we encounter a high free energy barrier separating this configuration from the ordered state, thus making the transition unlikely to occur in a simulation run on a reasonable time scale. However, on large time scales such an event will occur. We will first take a look at the reason for the formation of domain boundaries in a system and then introduce the Wang-Landau [27]

algorithm which can be used to determine the significance of domain formation for the low temperature phase of our model.

The formation of domains cannot be explained unless the density of states is taken into account. Lattice configurations with separate domains are not the energetic ground state of the system but their higher degree of degeneracy could make these configurations the state with the lowest free energy. The probability to find a system in a certain state  $\nu$ , i.e., spin configuration, is given by

$$p_\nu = \frac{e^{-\beta E_\nu}}{Z}, \quad (3.1)$$

where  $Z$  is the canonical partition function

$$Z = \sum_\nu e^{-\beta E_\nu}, \quad (3.2)$$

where the sum is taken over all configurations of spins on the lattice. When we are interested in a group of states, such as states with a certain energy, we have to take into account how many of these spin configurations have identical energies.

Introducing the density of states  $g(E)$ , which is the degeneracy of the energy  $E$ , we obtain the probability to find the system in a state with energy  $E$

$$p(E) = \frac{g(E)e^{-\beta E}}{Z}. \quad (3.3)$$

The contribution of the density of states can be interpreted as an entropic term which depends on the size of the system. The behavior of the system in the thermodynamic limit depends on the relationship between the increase in the energy of the states in the limit  $N \rightarrow \infty$  and the increase in configuration space volume.

In order to analyze the importance of the density of states for the behavior of our system, we want the system configurations sampled during simulations to be as broadly distributed in configuration space as possible. We will make use of an algorithm devised by Wang and Landau [27], which is designed to cross high barriers in the free energy landscape of a system thus sampling a large volume in configuration space.

Although the Wang-Landau algorithm, also known as flat histogram sampling, was originally used to calculate the microcanonical density of states, it has been successfully applied to obtain probability distributions for reaction coordinates [28]. As a result of a simulation run, the free energy profile of the system can be obtained with remarkably reduced computational cost in comparison to Metropolis Monte Carlo simulation.

The general idea of the algorithm is to find an accurate estimate for the density of states via a simulation which produces a flat histogram. Instead of using the Boltzmann weight as the criterion whether moves are accepted or rejected, we define a different Hamiltonian for the system:

$$H = H' + W(\eta) , \quad (3.4)$$

where  $H'$  is the original Hamiltonian.  $W(\eta)$  is initially set to zero for all values of  $\eta$  and every time the system visits a state with an order parameter value  $\eta_i$ ,  $W(\eta_i)$  is incremented by a modification term  $f > 0$ .  $W(\eta)$  is constantly changed by these increments and each visit of a state with an order parameter value  $\eta_i$  makes it less likely that a state with  $\eta = \eta_i$  is visited again. Consequently, the system is driven to regions in configuration space which have not been sampled during the run of the simulation.

The acceptance criterion for a state  $n$  if the system currently is in state  $o$  is given by

$$p(o \rightarrow n) = \min \{1, \exp(-\beta [\Delta E_{o \rightarrow n} + \Delta W_{o \rightarrow n}(\eta)])\} \quad (3.5)$$

where

$$\begin{aligned} \Delta E_{o \rightarrow n} &: = E_n - E_o \\ \Delta W_{o \rightarrow n} &: = W(\eta_n) - W(\eta_o) . \end{aligned} \quad (3.6)$$

As the simulation proceeds, the states of the system are biased depending on their value of  $\eta$ . The modification factor  $f$  is decreased over time until it reaches zero. At this point  $W(\eta)$  is a good estimate for the Landau free energy

$$W(\eta) \approx -F(\eta) \propto k_B T \ln [p(\eta)] \quad (3.7)$$

where

$$p(\eta) = \sum_{\nu} p_{\nu} \delta_{\eta \eta_{\nu}} \quad (3.8)$$

is the probability distribution for the order parameter  $\eta$ .

The implementation of this algorithm is surprisingly simple, especially for models with discrete order parameters. During the simulation run two histograms over the range of the order parameter are created, both initially set to zero for all values of  $\eta$ . The bin size of the histograms is given by the smallest discrete changes in the order parameter and the possible values for  $\eta$  range from  $-1$  to  $1$ . One of these histograms is  $W(\eta)$  which is incremented by  $f$  every time the system is in a configuration with an order parameter  $\eta$ .

The second histogram is increased by a constant factor for each visit and therefore becomes flat with increasing time because the energetically favored states are biased unfavorably by  $W(\eta)$ .

As soon as the histogram of visited values of  $\eta$  fulfills a flatness criterion, it is reset and the modification factor  $f$  is decreased. Repeating this step refines the histogram of  $W(\eta)$  and the simulation run is continued until the increment is so small that the changes in  $W(\eta)$  are negligible.

Using flat histogram sampling also helps decreasing the effect of critical slowing down [27] in the vicinity of the critical point of the system, because the bias drives the system from one peak in the probability distribution to the other. For the system sizes investigated we achieved sufficient sampling of configuration space in the vicinity of the critical point.

If one is interested in the simulation of much larger systems, it might still be necessary to introduce an algorithm which is by design highly resistant towards critical slowing down effects, i.e., cluster flip algorithms [29]. However these algorithms come with their own disadvantages which will not be discussed in this work.

## 3.2 Biased Sampling

Wang-Landau sampling is used in our simulation to determine the free energy profile as a function of the order parameter  $\eta$ , which in turn contains all the information to obtain the probability density  $p(\eta)$

$$p(\eta) \propto \exp[-\beta F(\eta)] . \quad (3.9)$$

The disadvantage of the algorithm is that the majority of computation time is spent simulating a system with a different and constantly changing Hamiltonian. If a sample of equilibrium configurations of the system is needed, it cannot be obtained by flat histogram sampling. During the simulation run the system is indeed not in equilibrium as the weight function in the acceptance criterion is permanently altered. Therefore the algorithm does not satisfy the detailed balance condition until the very end of simulation runs when the increment  $f$  is negligible<sup>1</sup> [28].

An efficient way to sample equilibrium configurations in our system, which we will need to perform histogram reweighting, is to implement biased sampling

---

<sup>1</sup>At this point, the algorithm fulfills detailed balance within an accuracy of the order of magnitude of  $f$ .

MC. As the name of the algorithm suggests, we introduce a bias function  $w(x)$ . The acceptance criterion for an MC trial move which brings the system from the old state  $o$  to the new state  $n$  is now given by [25]

$$acc(o \rightarrow n) = \min \left\{ 1, \frac{w_o(x)}{w_n(x)} \exp(-\beta [E_n(x) - E_o(x)]) \right\} . \quad (3.10)$$

Our goal is to sample configurations which cover the whole range of the order parameter  $\eta$  which leads us to

$$acc(o \rightarrow n) = \min \left\{ 1, \frac{w(\eta_o)}{w(\eta_n)} \exp(-\beta (E_n - E_o)) \right\} . \quad (3.11)$$

Obviously, the average value of the above acceptance criterion is an indicator for the efficiency of the algorithm, because rejected trial moves do not propagate the system in state space. It is possible to improve the acceptance rate significantly by choosing

$$w(\eta) = \frac{1}{p(\eta)} = \exp(-\ln [p(\eta)]) = \exp[\beta F(\eta)] . \quad (3.12)$$

Thus equation (3.11) becomes

$$acc(o \rightarrow n) = \min \{ 1, \exp(-\beta [\Delta E_{o \rightarrow n} + \Delta F_{o \rightarrow n}(\eta)]) \} \quad (3.13)$$

where

$$\begin{aligned} \Delta E_{o \rightarrow n} : &= E_n - E_o \\ \Delta F_{o \rightarrow n} : &= F(\eta_n) - F(\eta_o) . \end{aligned} \quad (3.14)$$

Therefore, Wang-Landau sampling provides us with the ideal weight function for our biased simulation.

The distribution of the sampled states needs to be treated in a way that restores the distribution one would obtain in an unbiased simulation. If we denote the distribution obtained from the biased simulation by  $p_w(\eta)$ , unfolding of the bias is given by

$$\begin{aligned} p(\eta) &\propto \frac{p_w(\eta)}{w(\eta)} \\ &\propto e^{\beta F(\eta)} p_w(\eta) . \end{aligned} \quad (3.15)$$

Evidently, the chosen weight function only affects the quality of the sampling and therefore the computational efficiency of the simulation but not the obtained distribution functions. Even if the weight function obtained by flat histogram sampling is not very accurate in terms of its statistics, biased sampling is suitable to refine the weight function, and thus our estimate for  $F(\eta)$ , efficiently.

If the weight function is chosen well, this algorithm achieves high computational efficiency and its sampling is evenly distributed in configuration space. After correcting for the introduced bias, one obtains equilibrium configurations of the system which makes this method perfectly suited to obtain data for histogram reweighting.

### 3.3 Histogram Reweighting

The histogram reweighting algorithm developed by Ferrenberg and Swendsen [30] is a powerful tool that is widely used to save computational cost by extracting a maximum amount of data from each simulation run [31].

The algorithm is based on the idea that the knowledge of the probability distribution of an observable for a certain temperature  $T$  makes it possible to estimate the probability distribution of this observable at a different temperature  $T'$ .

A histogram  $H_\beta(E, \eta)$  obtained from a simulation at an inverse temperature  $\beta$  naturally suffers from statistical errors, but it is a good estimate for  $p(\beta, E, \eta)$ :

$$\frac{H_\beta(E, \eta)}{N} = \frac{1}{Z(\beta)} \exp(-\beta E) g(E, \eta) \quad (3.16)$$

where  $N$  is the number of entries in the histogram and  $g(E, \eta)$  is an estimate for the true density of states [32]. Now we can insert

$$g(E, \eta) = \frac{Z(\beta)}{N} \exp(\beta E) H_\beta(E, \eta) \quad (3.17)$$

into the original definition of  $p(\beta, E, \eta)$

$$p(\beta, E, \eta) = \frac{g(E, \eta) \exp(-\beta E)}{\sum_E g(E, \eta) \exp(-\beta E)} \quad (3.18)$$

where  $g(E, \eta)$  is the true density of states.

We find that an estimate for the probability distribution  $p(\beta', E, \eta)$  for an arbitrary inverse temperature  $\beta'$  is given by

$$p(\beta', E, \eta) = \frac{H_\beta(E, \eta) \exp[(\beta - \beta')E]}{\sum_E H_\beta(E, \eta) \exp[(\beta - \beta')E]} \quad (3.19)$$

Therefore the probability distribution  $p(\beta, E, \eta)$  can be reweighted to an inverse temperature  $\beta'$ .

In order to find the critical point for a certain system configuration by comparison with the distribution function of the matching universality class<sup>2</sup> one has

<sup>2</sup>Please refer to Sec. 4.3 for details.

a narrow range of temperatures where the desired probability density is produced. In order to avoid multiple simulations within this narrow spread of temperatures we implemented histogram reweighting, thus reducing computational cost significantly [33].

If one obtains the histograms in a Metropolis MC simulation, the range of temperatures where histogram reweighting can be carried out is limited by the quality of the sampling. If the portion of configuration space sampled at temperature  $T$  does not overlap sufficiently with the part of configuration space sampled at  $T'$ , the reweighting will not be successful. Since we have obtained our data from a biased simulation in which every value of  $\eta$  is equally probable, thus greatly enhancing the sampling of configuration space, we are confident that the range of temperatures accessible by reweighting is widened. However, as for all sets of parameters we investigated the vicinity of  $T_c$  was roughly known from preliminary calculations, it was not necessary to perform histogram reweighting over a large range of temperatures.

### 3.4 Finite Size Effects

The box of particles where the simulation is executed is finite, in fact due to restrictions in computational cost it is often small in comparison to the system it is supposed to mimic. There are several methods available to avoid unphysical surface effects which would not occur in a system of macroscopic size. The choice of method crucially depends on the range of the interaction in the model which will be treated in Subsection 3.4.1. The approach we used based on these considerations will be presented in Subsection 3.4.2.

#### 3.4.1 Range of the Interaction Potential

The properties of the membrane are crucially influenced by the nature of the interaction between the water wires. As we explained in Sec. 2.2, the water molecules are modeled as point dipoles and the interaction potential  $\Psi(\mathbf{r}_{ij}, \mathbf{p}_i, \mathbf{p}_j)$  between two molecules  $i$  and  $j$  is given by Eq. 2.2. We will study the dependence of the interaction energy of one dipole with all other dipoles on the lattice on the cutoff radius  $r_c$ .

The size of the interaction range is of extraordinary importance for the modelling of the system. If the interaction is of short range, we can introduce a cutoff  $r_c$  and, for each particle, neglect the interaction energy for larger distances  $r > r_c$ . We will analyze the dependence of the interaction energy per particle on  $r_c$  with

the constraint

$$\mathbf{p}_i = \mathbf{p}_j = \begin{pmatrix} 0 \\ 0 \\ \mu \end{pmatrix}. \quad (3.20)$$

This constraint guarantees that contributions to the interaction energy will not cancel.

In a bulk system in three dimensions with a density  $\rho(r)$ , the number of particles  $\Delta N$  contained in a spherical shell of thickness  $\Delta r$  is

$$\Delta N = 4\pi\rho r^2\Delta r. \quad (3.21)$$

Thus the systematic error in the interaction energy per particle in three dimensions resulting from the introduction of a cutoff is given by

$$Err = 4\pi \int_{r_c}^{\infty} \rho(\mathbf{r}) \Psi(\mathbf{r}_{ij}, \mathbf{p}_i, \mathbf{p}_j) r^2 d\mathbf{r}. \quad (3.22)$$

The systematic error introduced by the cutoff converges if and only if the interaction decays fast enough for large distances compared to the increase in the number of particles per shell. The error introduced by using a finite cutoff for dipole-dipole interactions in a three dimensional bulk system diverges for the chosen constraint, as the integrand in Eq. (3.22) is of order  $r^{-1}$  for dipole-dipole interactions.

However, the system in question is not a three dimensional bulk system but a system with periodicity in two dimensions and a finite length, the thickness of the membrane, in the third. Thus, for large system sizes the thickness of the membrane is small compared to the other dimensions and the geometry resembles a quasi two dimensional structure. This implies that for large distances the number of interaction partners in the membrane increases proportionally to the lateral surface of a cylinder with height  $L$

$$\Delta N = 2\pi L\rho r\Delta r, \quad (3.23)$$

where  $L$  is the length of the tubes in the membrane, i.e., its thickness.

Consequently, the error introduced by the use of a cutoff in the interaction potential is given by

$$Err = 2\pi L \int_{r_c}^{\infty} \rho(\mathbf{r}) \Psi(\mathbf{r}_{ij}, \mathbf{p}_i, \mathbf{p}_j) r d\mathbf{r}. \quad (3.24)$$

The leading term in the integrand is of order  $r^{-2}$  for dipole-dipole interaction (2.2) and the error is therefore finite.

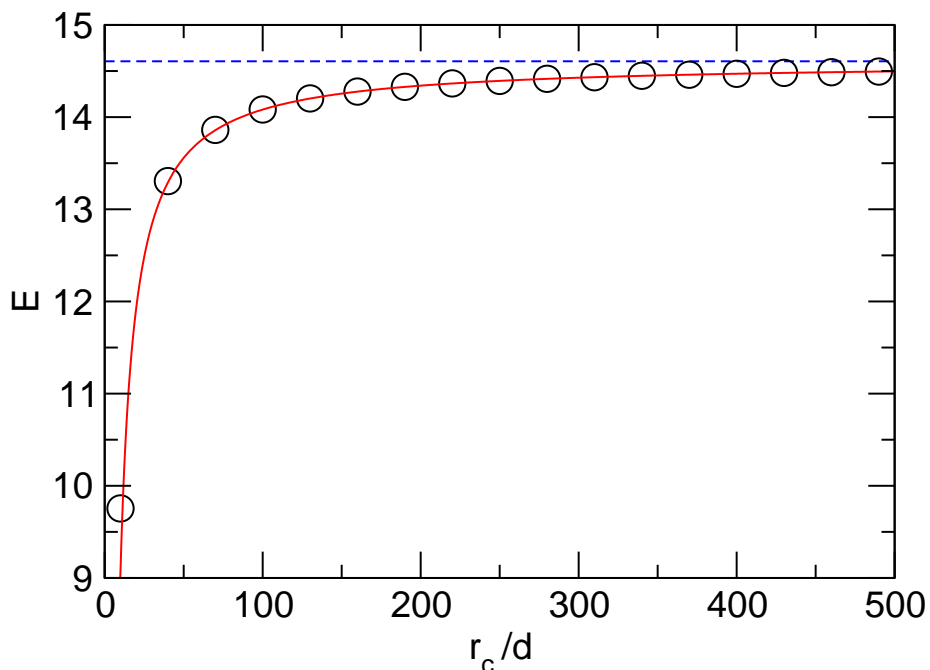


Figure 3.1: Interaction energy per tube  $E$  as a function of  $r_c/d$ . Circles indicate numerical results, showing good agreement with the function  $\propto A_0 - A_1/r$  shown as a red line. The function value in the limit  $r_c \rightarrow \infty$  is depicted by the dashed blue line.  $E$  is given in reduced units.

The energy per particle in the system for a given cutoff  $r_c$  should have the functional form

$$\begin{aligned}
 \frac{1}{N} \sum_{(i,j)} \Psi(\mathbf{r}_{ij}, \mathbf{p}_i, \mathbf{p}_j) &\propto \int_d^{r_c} r \Phi(r) dr \\
 &\propto \int_d^{r_c} \frac{1}{r^2} dr \\
 &\propto \frac{1}{r}
 \end{aligned} \tag{3.25}$$

in Gaussian units, where  $N$  is the number of point dipoles in the system.

To evaluate the quality of our assumption we calculated the interaction energy per tube for different values of  $r_c$ . The interaction energy per tube is proportional to the mean interaction energy per dipole in the tube with the advantage that we do not have to concern ourselves with the question how the particle's position in the tube affects the magnitude of its interaction energy. The system contains  $980 \times 980$  tubes with 32 water molecules each with a spacing of  $a = 2.65 \text{ \AA}$  between the dipoles in the tube and a tube spacing of  $d = 13.25 \text{ \AA}$ .

We varied  $r_c$  from  $26.5 \text{ \AA}$  to  $1298.5 \text{ \AA}$ . To avoid the effect of errors cancelling each other, we kept all of the molecules on the lattice pointing in the same

direction. Fig. 3.1 shows the numerical results for the interaction energy of one tube with all other tubes in the membrane as a function of the cutoff radius. The graph clearly shows that the predicted function fits the interaction energies very well, even for small cutoffs.

Hence we conclude that the tubes on the lattice are coupled to each other via short ranged interactions.

### 3.4.2 Multiple Image Convention

In order to increase the computational efficiency of simulations, the box in which the simulation takes place is often small compared to the system it models. This is especially troublesome for simulations of bulk material where this small simulation box leads to strong surface effects in simulation, while the influence of surface effects for bulk material is negligible. Such surface effects are undesirable and one strives to avoid them in simulation.

In many if not most cases the instrument of choice to overcome these effects are periodic boundary conditions. In this method the simulation box is interpreted as the primitive cell of an infinite periodic lattice. The interaction  $\Phi_{ij}$  of two water chains  $i$  and  $j$  with a distance vector  $\mathbf{R}_{ij}$  in a simulation box of length  $\lambda$  is then given by [25]

$$\Phi_{ij} = \sum_{\mathbf{n}} \Phi(|\mathbf{R}_{ij} + \mathbf{n}\lambda|) , \quad (3.26)$$

where  $\mathbf{n}$  is an arbitrary vector of integers. As our system is periodic in two dimensions we only apply the periodic boundary conditions in these dimensions and the z-component of  $\mathbf{n}$  is always zero. Obviously, calculating the interactions on this infinite lattice would require us to evaluate infinite sums. As this can be a troublesome procedure itself, one usually chooses a convention to select the interaction partners for any given particle depending on its position.

The most common choice is the nearest image convention (NIC). Using the NIC, a spherical cutoff of length  $\lambda/2$  is introduced and only tubes within this cutoff radius are accounted for in the calculation. The interaction energy between two tubes is then computed as the interaction between a tube and the other tube's nearest image. The interaction between two tubes is given by equation (3.26) with the restriction

$$|\mathbf{R}_{ij} + \mathbf{n}\lambda| < \frac{\lambda}{2} \quad (3.27)$$

From a different point of view, the interaction between tube  $i$  and all other tubes in the system is calculated within a sphere of diameter  $\lambda$  which is centered around tube  $i$  on the infinite lattice created by the periodic boundary conditions.

If we want to consider the applicability of this method to our model we have to remind ourselves of the spatial properties of our system. The membrane has a finite thickness which is small compared to its dimensions in the lateral directions and we want our simulation box to resemble this shape. This instantly leads to complications if the NIC is used. If the spatial characteristics of the system are to be reflected by our model, the simulation box has to be of a size that makes the thickness of the membrane small against the other dimensions. This leads to simulation boxes of proportions which are not accessible in simulations within the boundaries of reasonable computation time.

Summing up the requirements for the boundary conditions in our system we need a method which allows us to model the spatial properties of the system while still keeping our simulation box at a manageable size. One way to achieve this is Ewald summation [34], which has the advantage of being applicable to long range interactions. We have shown before that the interactions in our system are of short range and therefore, if at all possible, we want to avoid dealing with the complications of performing Ewald summation on a slab geometry [35, 36].

As a consequence of these considerations, we implemented the multiple image convention. We still use periodic boundary conditions in two dimensions, thus replicating the simulation box infinitely in space, but we choose to include multiple images of the tubes into the calculation of the interaction energy. The interaction energy between two chains is given by equation (3.26) with the restriction

$$|\mathbf{R}_{ij} + \mathbf{n}\lambda| < \frac{m\lambda}{2}, \quad (3.28)$$

where  $m$  is the number of mirror boxes accounted for in each dimension.

Utilizing the fact that the particles have fixed positions on the lattice we can avoid to calculate the interactions of all the mirror boxes at each step of the simulation. At the start of each run we calculate the interaction energies between the chains for all distances in the simulation box, including the interaction with all the particle images in the mirror boxes. Now the interaction energy between any two chains in the box is determined up to the orientation of the dipole moment. The interaction energies  $\Phi_{ij}$  are tabulated and for each calculation of the interaction energy in the simulation, the computational cost is reduced to multiplying the value of the interacting spins with the tabulated interaction energy.

Therefore, during the simulation we retain the computational efficiency of our comparatively small simulation box. At the same time the larger cutoff, which includes many mirror boxes of our simulation box, lets our interaction closely

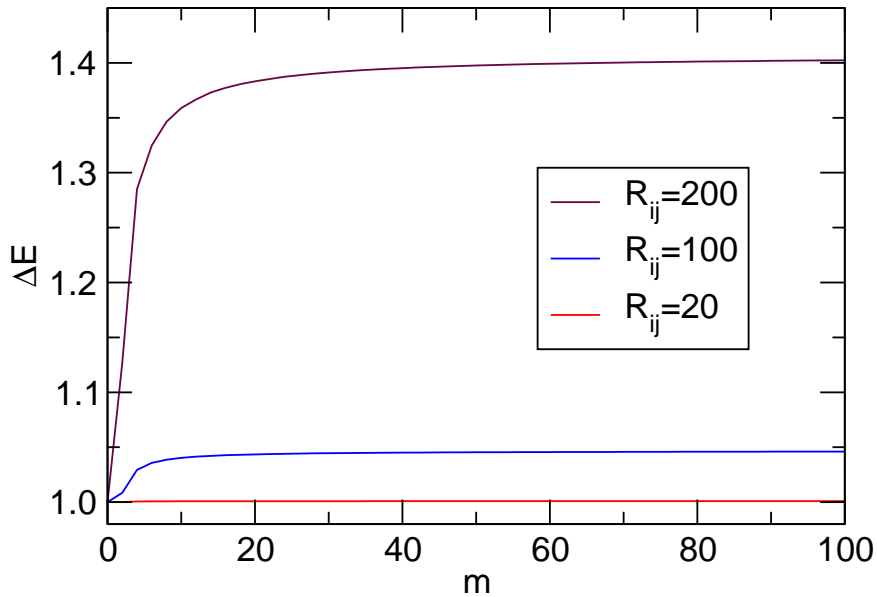


Figure 3.2: Relative change in the interaction energy  $E$  between two tubes at a distance  $R_{ij}$  as a function of the number of included mirror boxes  $m$  in each direction for a lattice with  $L = 32$  and  $d = 20$ .

resemble the geometric properties of a bulk membrane.

The effect of the inclusion of the mirror boxes in the computation of the interaction energy on a lattice with  $N = 900$  tubes is depicted in Fig. 3.2. We calculated the change in the interaction energy divided by the interaction energy for  $m = 0$ . For two tubes in close proximity on the lattice the relative change in  $E$  by the inclusion of the mirror boxes is negligible as the interaction with the chain in the simulation box is very large compared to the contributions of the mirror chains. However, for two chains at a larger distance in the simulation box, the interaction changes considerably by the inclusion of the mirror chains. The change in interaction energy for the chosen lattice parameters declines for  $m \gtrsim 20$ . We will study the effect of this change in interaction energies on the obtained critical temperatures in Sec. 4.5.

With the advantage of high computational speed we also have to accept the shortcomings of a simulation in small simulation box. By replicating our small box we only allow the system fluctuations with a wavelength compatible with the periodic lattice [25]. In particular, the maximum wavelength of fluctuations is the length of the simulation box which will distort the system behavior in the vicinity of the critical point, where the correlation length grows rapidly.

## Chapter 4

# Numerical Results

We will start this Chapter with a short section about the “tricks of the trade” we use to obtain data from our simulations and then introduce the units used throughout this Chapter.

In the following Section we will study the importance of domain building for the phase behavior of our system. The implementation of Wang-Landau sampling avoids that the system gets trapped in a metastable state and allows us to study its free energy profile.

We treated the subject of finite size effects in the previous Chapter, but boundary effects are unfortunately not the only difficulties that arise from our small simulation box. By definition, phase transitions only take place in the thermodynamic limit and it is a challenging task to correct for effects which influence the data obtained from simulations in a system of finite size. The method used in this work to determine the critical point is a comparison with the behavior of systems belonging to the same universality class which will be introduced in Sec. 4.3. Using this method, we study the influence of system size and the multiple image convention on the obtained estimate for the critical temperature in Sections 4.4 and 4.5.

Subsequently, we investigate the accuracy of the estimates for the critical point of corresponding states of the membrane, obtained by the relations derived in Sec. 2.4. Taking these results into consideration, we obtain a phase diagram for membranes with different ratios between tube length and tube spacing in the final Section of this Chapter.

## 4.1 Technical Aspects

In this Section we will give a short overview of the technical details involved in our simulations and in data processing.

All lattice configurations are quadratic and the tubes are parallel to each other. The spatial configuration of the lattice is determined by the length of the tubes  $L$  and the lattice spacing  $d$ , which is the distance between a tube and its nearest neighbours.

The single-file water chains are ordered, hence the problem is reduced to a two dimensional lattice with a distance dependent coupling constant  $\Phi(\mathbf{R}_{ij})$  defined in Eq. (2.4). These interaction energies are calculated for the fixed lattice positions using the multiple image convention and are subsequently tabulated. This computation is executed in `long double` precision in order to keep the numerical errors resulting from adding many small values to a number of higher magnitude at bay. We use these tabulated interaction energy values in all following calculations for this spatial configuration of the lattice.

In the next step we find a temperature in the vicinity of the critical point via analysis of the free energy curves as a function of the order parameter obtained by Wang-Landau sampling. The free energy profile for this temperature is then used in a biased Monte Carlo simulation where  $1.4 \times 10^7$  sweeps, i.e.,  $N$  Monte Carlo trial moves where  $N$  is the number of tubes in the system, are computed. The obtained histograms are then reweighted to locate the critical point of the system using the technique described in Sec. 4.3.

Throughout the simulation reduced units are used for convenience. The unit of length is the spacing between the dipoles in the tubes  $a = 2.65 \text{ \AA}$ . The length of single-file water chains  $L$  is then equal to the number of particles residing in the tube. The dipole moment is given in units of the average dipole moment in direction of the tube axis of a single point dipole representing a water molecule in the chain  $\mu = 1.9975 \text{ D}$ . If we insert these units into the dipole-dipole interaction from Eq. (2.2)

$$\begin{aligned} \Psi(\mathbf{r}_{ij}, \mathbf{p}_i, \mathbf{p}_j) &= -\frac{\frac{3}{a^2\mu^2}(\mathbf{r}_{ij} \cdot \mathbf{p}_i)(\mathbf{r}_{ij} \cdot \mathbf{p}_j) - \frac{1}{a^2\mu^2}r_{ij}^2\mathbf{p}_i \cdot \mathbf{p}_j}{\frac{r_{ij}^5}{a^5}} \\ &= -\frac{a^3}{\mu^2} \frac{3(\mathbf{r}_{ij} \cdot \mathbf{p}_i)(\mathbf{r}_{ij} \cdot \mathbf{p}_j) - r_{ij}^2\mathbf{p}_i \cdot \mathbf{p}_j}{r_{ij}^5} \end{aligned} \quad (4.1)$$

we obtain the reduced unit<sup>1</sup> of energy  $\varepsilon = \mu^2/a^3$ . This implies the unit  $1/\varepsilon$  for

<sup>1</sup>The unit of energy  $\varepsilon$  differs from the reduced unit of energy used in Ref. [3] which we shall denote here as  $\tilde{\varepsilon}$ . The relation is then given by  $\varepsilon = \tilde{\varepsilon}/2$ . Thus  $\tilde{\beta} = \tilde{\varepsilon}/(k_B T)$ .

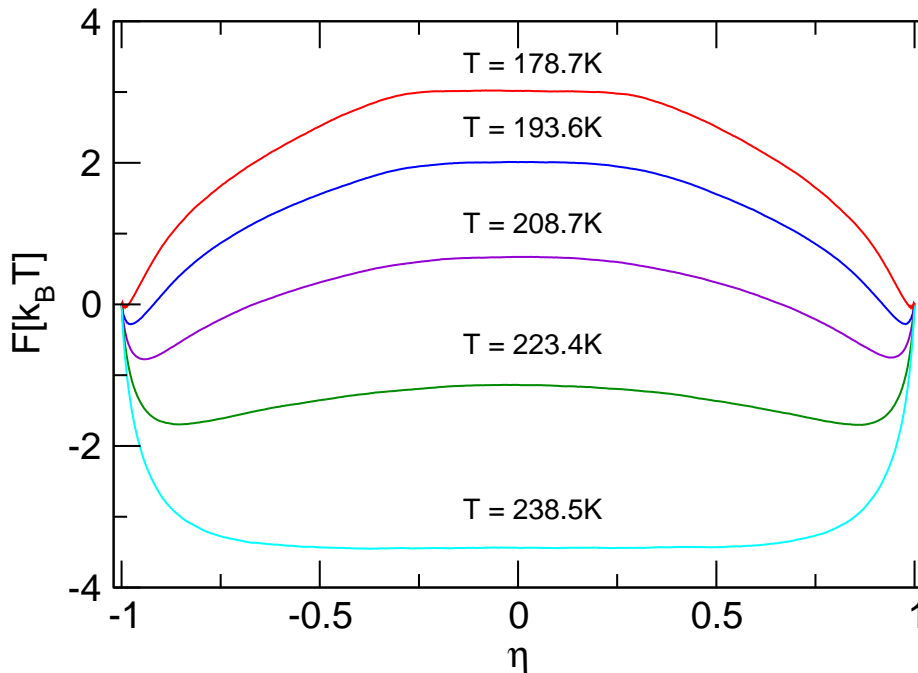


Figure 4.1: Free energy profile for a system containing 900 tubes of length  $L = 8$  with a lattice spacing  $d = 5$ . The free energies are symmetric about zero and the curves are shifted so that the free energy of the ordered state vanishes. It should be noted that these free energy curves are affected by finite size effects and thus are only suitable for qualitative analysis.

the inverse temperature  $\beta$ .

As reduced inverse temperatures are not a very intuitive measure, we shall express the temperature in units of K, unless stated otherwise.

## 4.2 Domains Revisited

When we introduced the order parameter for our system in Sec. 2.6, we were concerned about its inability to detect the formation of domains on the lattice. When phase separation occurs on the lattice, the contributions of each domain to the order parameter cancel, thus leading to low values of  $\eta$ . During some preliminary simulation runs using the Metropolis Monte Carlo algorithm [26], we noticed the formation of domains at low temperatures. One of the reasons for implementing the Wang-Landau algorithm was that it allows us to determine the true importance of this effect for the phase behavior of the system. Using Wang-Landau sampling we ensure that the system does not get stuck in a metastable state and we can determine the influence of configurations with separate domains

on the low temperature behavior of the system.

The free energy landscape depicted in Fig. 4.1 for various temperatures provides insight into the behavior of the system. For low temperatures we observe a high free energy barrier separating the two ordered states. For higher temperatures, the height of the barrier is diminished thus increasing the likelihood of crossings between the two ordered states due to thermal fluctuations. When the temperature is increased further, the barrier vanishes and the free energy has a minimum at  $\eta = 0$  corresponding to a likely disordered state.

A study of configurations with vanishing order parameter shows that states including domains of the antiferroelectrically ordered state are indeed sampled by the chosen methods. However, the analysis of the free energy curves indicates that the states in question are insignificant for the system behavior at low temperatures.

### 4.3 Universality Class

We aim to make predictions about the phase behavior of a water filled membrane with the data obtained from our simulations. However, the membrane is a macroscopic object and the simulation is performed in a comparatively small simulation box. Even considering that the interaction energies between the spins are calculated for much larger systems by use of the multiple image convention, this implies that the data obtained from the simulation might differ substantially from the behavior of the physical system investigated. In particular, phase diagrams directly obtained from simulations tend to yield estimates for the critical temperature which are too high (see Fig. 4.2) due to finite size effects.

This discrepancy will be substantial in the proximity of the critical temperature  $T_c$  which is the temperature range we are most interested in. To understand how to deal with this difficulty we will take a look at the concept of universality classes.

The basic idea behind universal behavior is that systems with different Hamiltonians show identical behavior at the critical point. Specifically, derivatives of the thermodynamic potentials exhibit power law behavior in the vicinity of a critical point of the system. Subsequently it is possible to define a set of critical exponents for the system and systems with identical critical exponents are considered as part of the same universality class [37].

A function  $f(\tau)$  of the reduced temperature

$$\tau = \frac{T - T_c}{T_c} \quad (4.2)$$

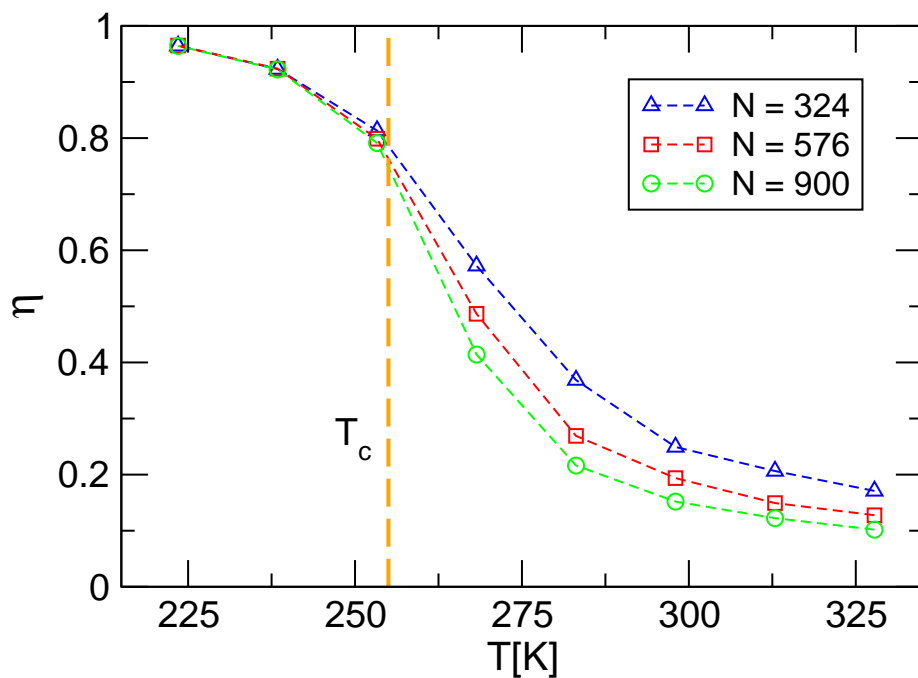


Figure 4.2: Order parameter  $\langle \eta \rangle$  as a function of temperature  $T$  for different system sizes obtained by computing the average of the order parameter distribution for  $\eta > 0$ . Each curve was computed for a lattice of tubes containing 32 particles each with a tube spacing of  $d = 5$ . While the agreement for low temperatures is good, finite size effects lead to differing values for higher temperatures. The orange line depicts  $T_c$  obtained by the method to be introduced later in this Section.

for  $\tau \rightarrow 0^+$  shows the scaling behavior [38]

$$f(\tau) \sim \tau^\lambda \quad (4.3)$$

with  $\lambda$  as the critical exponent. In the vicinity of  $T_c$  corrections to this pure scaling behavior are to be expected.

Properties which influence the critical exponents of a system are known to include the symmetry of the lattice, interaction range, spatial dimension and symmetry of the ordered state [32]. If the properties of our model are compared to those of the quadratic two-dimensional Ising model, one notices strong similarities:

- Range of the interaction:

In Subsection 3.4.1 we have shown that the energy per particle in our model remains finite in the limit  $N \rightarrow \infty$ . Therefore the interaction is of short

range which is evidently the case for the Ising model, which includes nearest-neighbour interactions only.

- System dimensions:

The width of the membrane is negligible for large membranes which makes it feasible to assume that it can be treated as a two dimensional system. This assumption is strongly supported by the results obtained in Subsection 3.4.1. In general, if the data is obtained by simulations in a finite system, the chosen boundary conditions lead to a universal shape and symmetry parameter [39]. For periodic boundary conditions however, this parameter is unity.

- Symmetry of the ordered state:

The ground state of the two models is identical and consequently both share  $\mathbb{Z}_2$  symmetry.

Hence we infer that our model belongs to the two-dimensional Ising universality class. This insight provides us with a powerful tool to determine the critical temperature  $T_c$  of our model to high accuracy.

For two systems belonging to the same universality class, the distribution

$$p(\bar{\eta}) := p\left(\frac{\eta}{\langle\eta^2\rangle}\right) \quad (4.4)$$

is identical at the critical point. Utilizing this we can obtain the critical temperature for our configuration by comparing  $p(\bar{\eta})$  in our system with the universal fixed point order parameter distribution for the appropriate universality class [33] shown in Fig. 4.3<sup>2</sup>. The best match between the order parameter distribution in simulation and the corresponding universal form is determined by minimizing the quadratic deviations between the two curves. This method has been successfully applied in the study of binary mixtures [40, 41].

In simulation, histogram reweighting allows us to produce order parameter distributions of our system for different temperatures without additional computational effort. Therefore, we can precisely locate the temperature at which the order parameter distribution in our model most closely resembles the universal order parameter distribution at the critical point.

This temperature is the critical temperature  $T_c$  of the system without corrections to the scaling behavior given by Eq. (4.3).

---

<sup>2</sup>We thank N. B. Wilding for generously providing us with the data for the universal order parameter distribution which were used in Ref. [39].

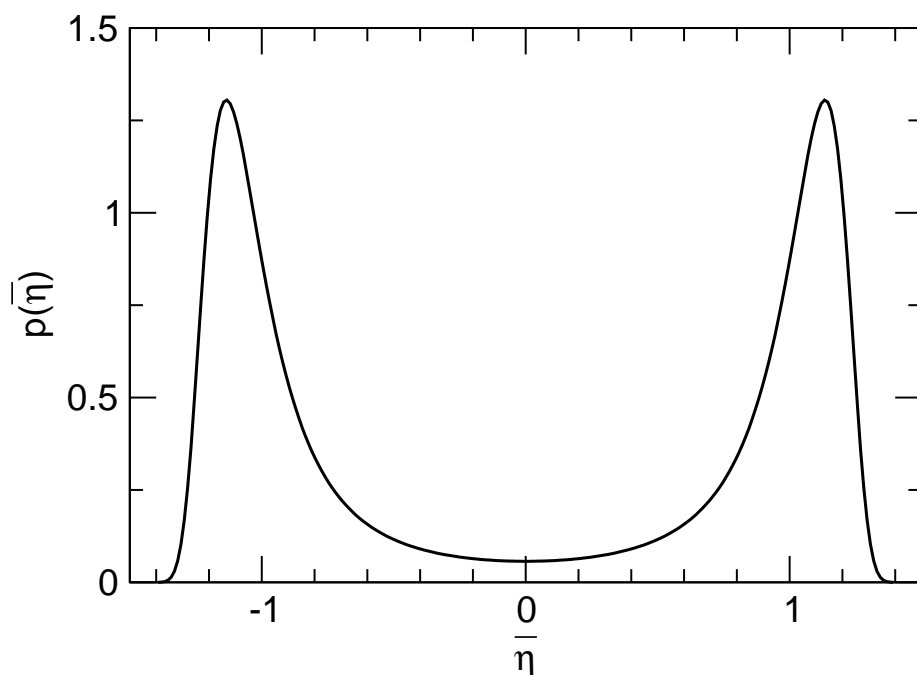


Figure 4.3: The universal fixed point order parameter distribution of the quadratic two-dimensional Ising model [39]. The distribution was scaled to unit variance.

In order to evaluate the suitability of this method to determine the critical temperature of our model, we will study the influence of finite size effects on the critical temperature obtained by this method. The significance of corrections to scaling behavior are determined in the following Sections by analyzing different system configurations.

#### 4.4 Influence of System Size on $T_c$

In order to determine the critical temperature for a given membrane we need to gain insight into the influence of the simulation box on the results obtained from our simulations. In this Section we investigate the influence of the simulation box size on the obtained values of  $T_c$ , determined by comparison of the order parameter distribution in simulation with the universal two-dimensional Ising order parameter distribution.

For reasons of computational efficiency one aims to keep the size of the simulation box as small as possible while still reproducing the quantities of interest obtained for larger model dimensions. Specifically, the computation time needed to perform a sweep of  $N$  trial moves in our biased Monte Carlo simulation is

roughly proportional to  $N^2$ , where  $N$  is the number of spins in the system.

To estimate the required size of the simulation box we choose a membrane with fixed tube length and tube spacing on the lattice and perform simulations using simulation boxes of different size, comparing the obtained estimates for the critical point.

We chose a membrane with a tube length  $L = 32$  and a tube spacing  $d = 20$ . The size of the simulation box was varied from 576 spins for the smallest system to 1600 for the largest. The simulations were performed at a temperature  $T = 55.88$  K which was known from preliminary calculations to be in the vicinity of the critical point.

The interaction energies for the distances on the lattice were tabulated and the free energy profile for the initial temperature was calculated by using flat histogram sampling. This free energy profile was then used in a biased simulation to create a histogram of the order parameter  $\eta$  and the corresponding energies of the configurations. The resulting histogram was reweighted in a range between  $T = 56.06$  K and  $T = 55.66$  K, subsequently scaled to unit variance and checked against the universal distribution of the order parameter. The comparison with the universal distribution at the critical point was performed by coarse graining the histograms  $p(\bar{\eta})$  and calculating the square error at 224 supporting points. The square deviations of the distributions obtained from simulations in the vicinity of  $T_c$  from the universal order parameter distribution are shown in Fig. 4.4. Corresponding order parameter distributions are depicted in Fig. 4.5. The resulting values for  $T$  in Fig. 4.6 have the smallest deviation from the universal distribution in the investigated temperature range and are therefore our estimates for  $T_c$  for the different system sizes.

Based on the results shown in Fig. 4.6, we conclude that the influence of system size on the critical temperature is negligible for the studied range of simulation box dimensions. While our estimate for  $T_c$  is lower for the largest system than for the other simulations, the difference is negligible. As a consequence, we will perform all subsequent simulations on a lattice with 900 spins, which reproduces the universal distribution with high accuracy and is still easily computationally accessible.

One should keep in mind that it cannot be expected to achieve results which are truly free of finite size effects by this method. In order to obtain this, a more sophisticated method like the Binder cumulants technique [42] is needed.

Still, based on the findings in this Section, we are confident that the dependence of the obtained critical points on system dimensions is not significant.

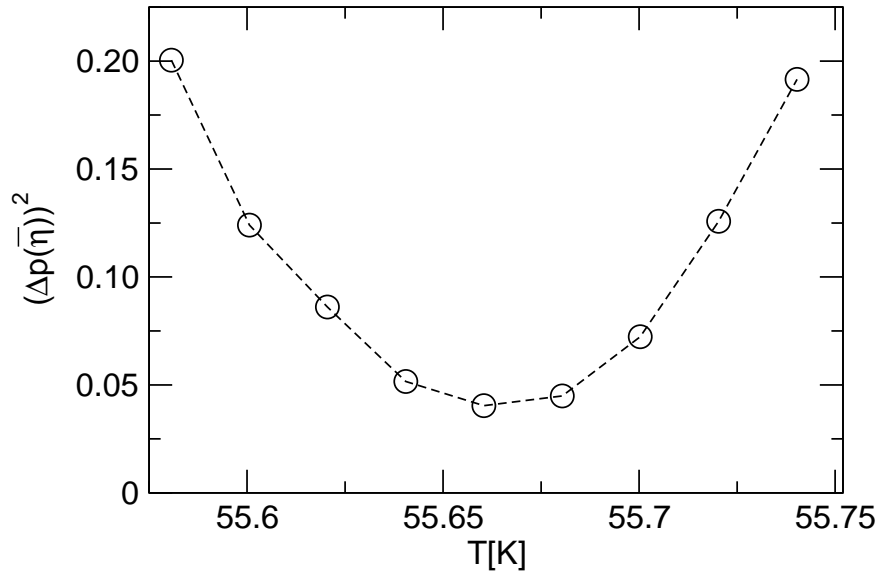


Figure 4.4: Square deviation of the distributions  $p(\bar{\eta})$  obtained for  $N = 900$  at different temperatures from the universal order parameter distribution at the critical temperature  $T_c$ .

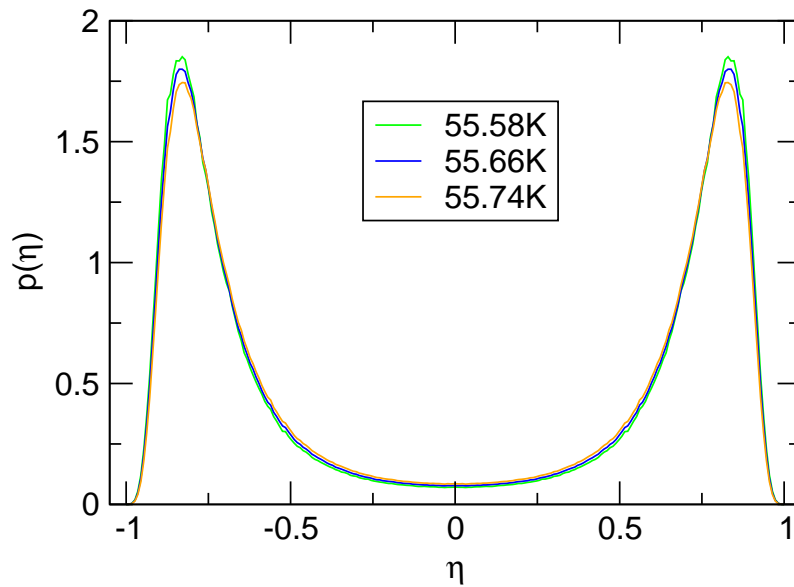


Figure 4.5: Probability distribution of the order parameter  $p(\eta)$ . The curve for  $T = 55.66\text{K}$  is the distribution at the critical temperature  $T_c$ . For lower temperatures, the peaks are more pronounced and the probability of the system crossing from one state to the other is decreased. For higher temperatures, we can see the opposite effect. These curves are not scaled to unit variance and are affected by finite size effects.

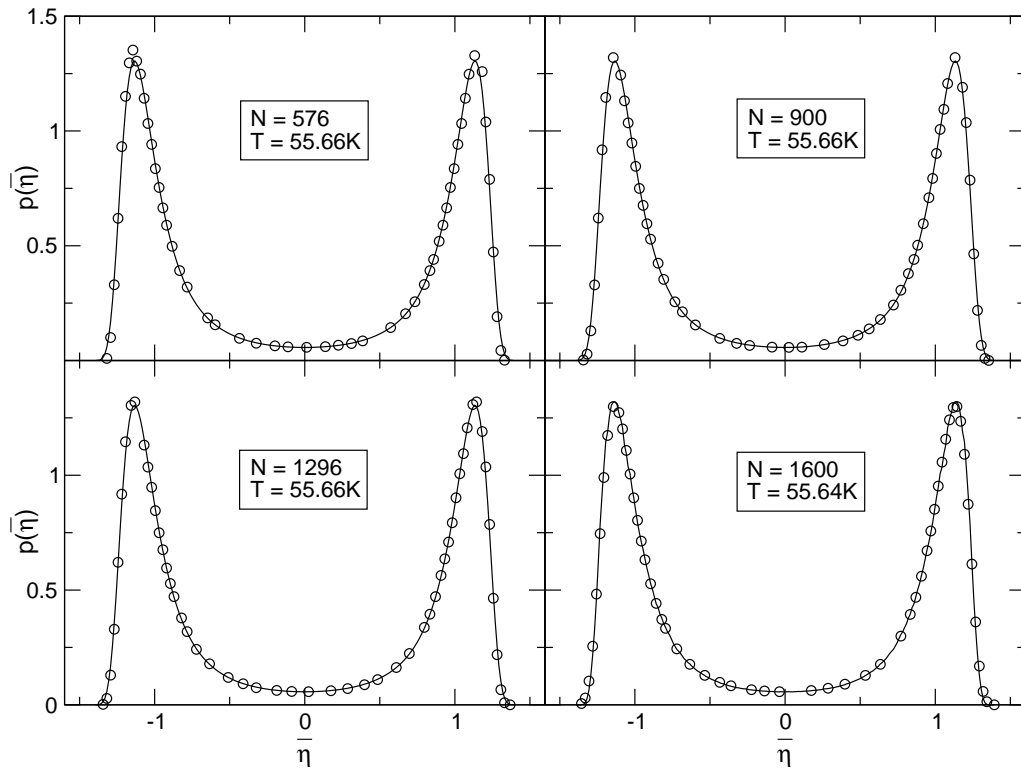


Figure 4.6: Numerical data obtained for different system sizes, indicated by circles, compared to the two-dimensional Ising universal fixed point order parameter distribution at the critical point, represented by the solid line. Our simulation results agree excellently with the universal order parameter distribution. The numerical results fit the reference curve better for increasing system size, but the overall error is small even for the simulation with 576 spins. Furthermore, the deviation of the numerical data from the universal distribution has little effect on the estimate for the critical point.

## 4.5 Parametrization of the Multiple Image Convention

In this Section we will investigate the influence of the number of “mirror boxes”  $m$  accounted for in the computation of the interaction energies on our estimate for the critical point of the system.

We performed simulations using a simulation box containing  $N = 900$  tubes with  $L = 32$  and a lattice spacing  $d = 20$ . The interaction potential  $\Phi(\mathbf{R}_{ij})$  was calculated by explicit dipole-dipole interaction (see Eq. (2.4)). The critical temperature was obtained by comparison of the order parameter distribution to its universal form at the critical point.

The results in Fig. 4.7 show that simulations using the multiple image convention yield a critical point different from data obtained by using the nearest image convention. This meets our expectations, as the spatial configuration of the membrane can be modelled more accurately using the multiple image convention, thus representing its “quasi-two-dimensional” properties. This also shows during the evaluation of the critical point, where the distribution function for the nearest image convention does not fit the universal distribution function as well as simulations where the multiple image convention was implemented. In

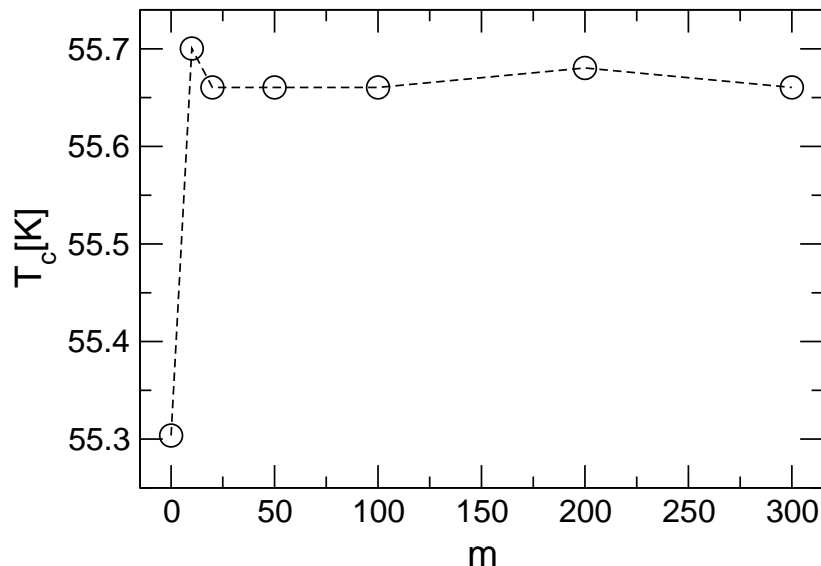


Figure 4.7: Critical temperature  $T_c$  as a function of the number of mirror boxes  $m$  included in the computation of the interaction energies. The value for  $m = 0$  corresponds to a simulation using the nearest image convention. The dashed line is a guide for the eye.

the studied system configuration only a small number of mirror boxes needs to be included in the computation of the interaction energies to reach the value of the critical point also obtained for larger  $m$ .

However, for tube lengths which are large in comparison to the tube spacing, we expect that more mirror boxes need to be included.

## 4.6 Corresponding States

In Sec. 2.4 we used the charge picture to obtain information about corresponding states on the lattice. In this Section we will compare the estimates for the critical point given by relation (2.22) to the values we obtained directly from simulation. As Eq. (2.22) is exact in the charge picture, any deviations of the estimates from simulation results will be induced by the numerical error of the charge picture approximation compared to the calculation performed in the dipole picture.

The simulations were performed in systems with a ratio between tube length and lattice spacing of  $L/d = 1.6$ . We performed multiple simulations with this ratio and varied the number of particles in the tubes from 8 to 128. In order to compare the obtained numerical results with our predictions, we need to choose one configuration as a starting point for the analytical estimates of the critical point.

To this end we computed the relative numerical error in the interaction of two tubes with length  $L$  and distance  $d$  computed in the charge picture compared to the interaction energy in the dipole picture:

$$\frac{\Delta\Phi}{\Phi} = \frac{\Phi_{ij}^{dipole} - \Phi_{ij}^{charge}}{\Phi_{ij}^{dipole}} \quad (4.5)$$

where  $\Phi_{ij}^{dipole}$  is defined according to Eq. (2.4) and  $\Phi_{ij}^{charge}$  according to Eq. (2.11).

The results in Fig. 4.8 show that the relative deviation between the dipole picture and the charge picture decays for longer chains for a constant ratio  $L/d$ . Consequently, we will choose the system with  $L = 128$  particles and  $d = 80$  as reference and compute the deviation from the analytical estimate for  $\beta_c$  when we decrease the length of the tubes in the system.

Based on the results shown in Fig. 4.9 we conclude that the system behavior agrees excellently with the predicted behavior. The deviation between the analytical prediction and the values directly obtained from simulation is too small to be seen in this graph.

However, using the method described in Sec. 4.3, we can detect deviations between the predicted values and the data obtained directly from simulation.

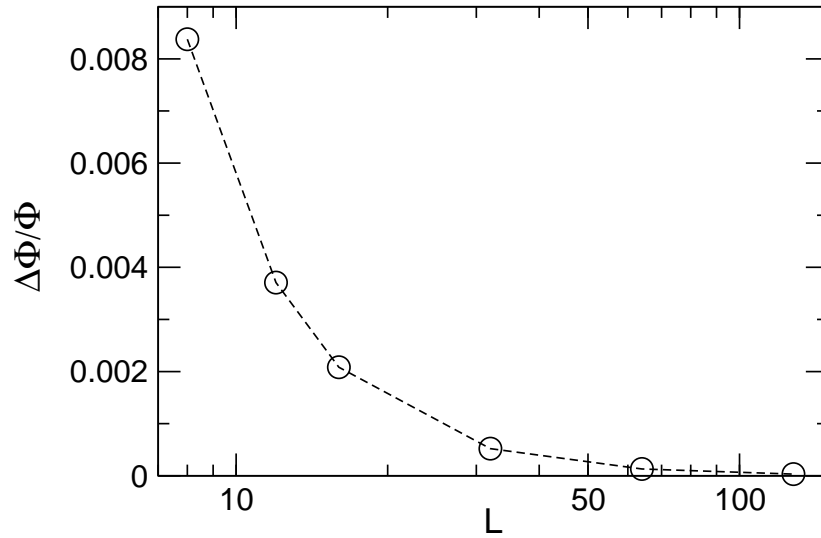


Figure 4.8: Relative error of the interaction between two tubes in the charge picture compared to the obtained value in the dipole picture. The ratio between the tube length and the lattice spacing of the tubes is constant at  $L/d = 1.6$ .

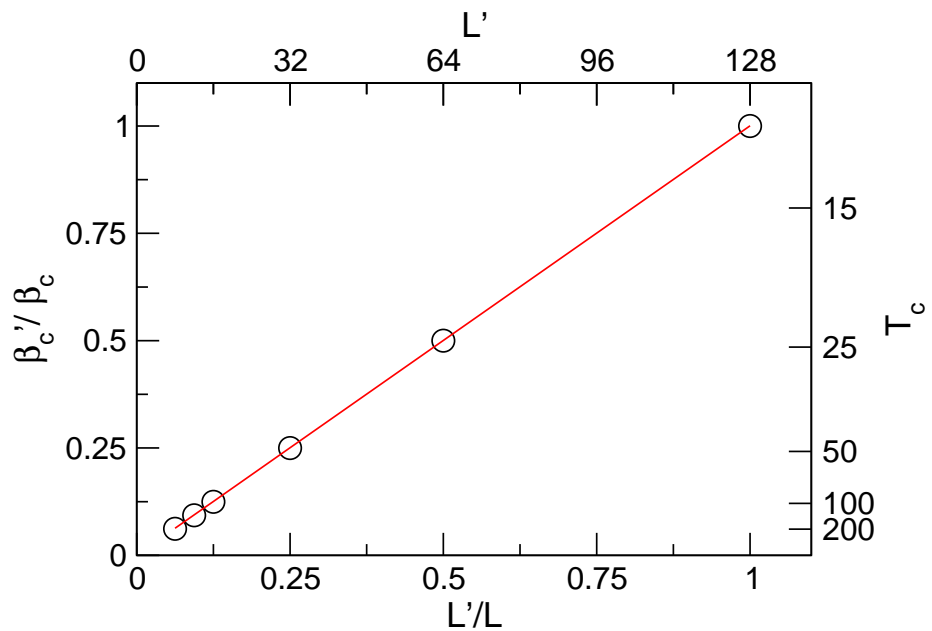


Figure 4.9: Numerical values (circles) for the different tube lengths  $L'$  with constant ratio  $L'/d'$ . The solid red line is the prediction from Eq. (2.22) with a slope of unity with respect to the bottom axis. The reference state is a system with  $L = 128$  and  $d = 80$ .

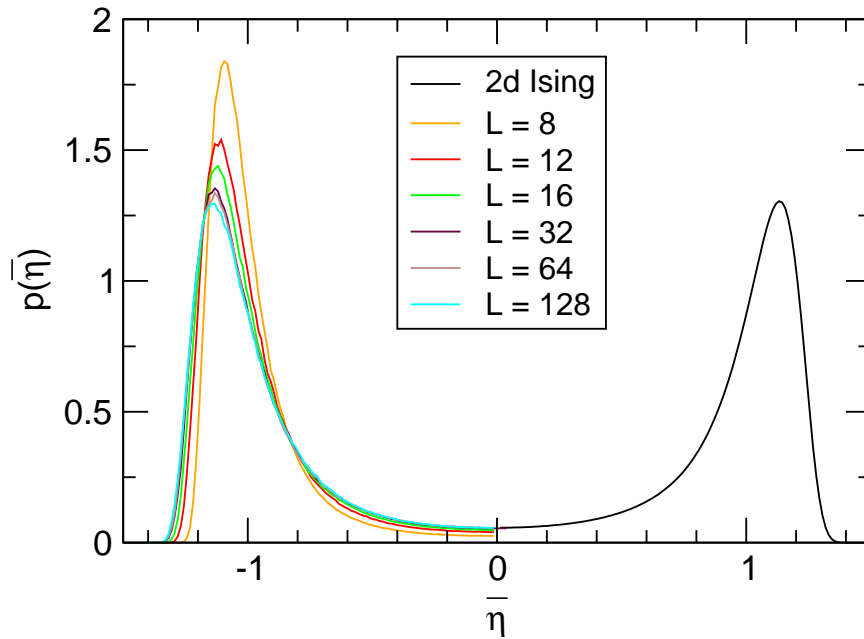


Figure 4.10: Distribution of the order parameter for various systems at the analytically predicted critical point based on  $T_c$  for the reference system with  $L = 128$ . Although the critical points obtained directly from simulation for the other systems deviate only marginally from the predicted values, the order parameter distributions of the systems at the predicted value for  $T_c$  differ substantially from each other. The solid black line is the universal order parameter distribution.

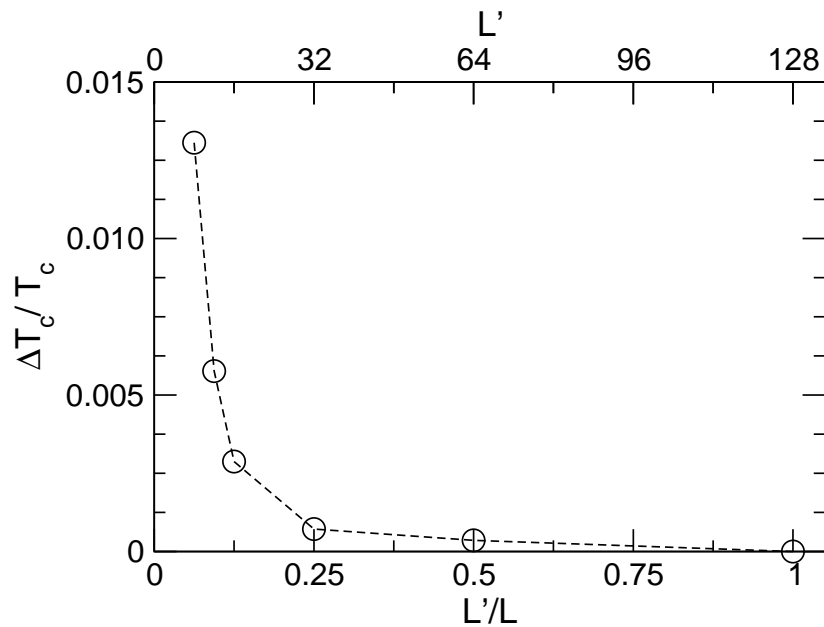


Figure 4.11: Relative error in the estimate for the critical point from Eq. (2.24) for each system.

The distribution functions for different tube lengths at the estimated critical point from Eq. (2.22) are shown in Fig. 4.10. This illustrates that the chosen method is very sensitive to small deviations from the predicted values and therefore well suited for a precise identification of the critical temperature.

The relative deviations of  $T_c$  directly obtained from simulation from the values  $T'_c$  predicted by Eq. (2.24)

$$\frac{\Delta T_c}{T_c} = \frac{T'_c - T_c}{T_c} \quad (4.6)$$

are small for all investigated tube lengths (see Fig 4.11), which does not come as a surprise due to the small deviation in interaction energies.

These results render the method of predicting the values of the critical point by use of Eq. (2.24) as highly accurate. Consequently, this method can be used to generalize the obtained results to a wide range of lattices with an identical ratio  $L/d$ .

## 4.7 Phase Diagram

In this Section we will present the obtained estimates for the critical point of lattices with different ratios between tube length and tube spacing. These results are manipulated by the analytic relations obtained in Sec. 2.4 to fit any membrane with an identical ratio  $L/d$ .

The data depicted in Fig. 4.12 show that all investigated membranes with a tube spacing of  $d = 10$  exhibit a critical point well below room temperature. The curve flattens for large tube lengths, leading to similar critical points for large values of  $L$ .

The flattening of the curve can be explained in the charge picture: When we keep the spacing between the tubes in the membrane constant and vary the length of the tubes, we alter the strength of the interaction between the diagonal charges at a distance  $r = \sqrt{L^2 + d^2}$ . If the two tubes in question are oriented in opposite directions and  $L$  is increased, the interaction between equal charges is decreased, which increases the strength of the coupling between the tubes. However, if the interaction with the diagonal charges is weak compared to the interaction with the charges at the same tube end, i.e., for  $L \gg d$ , increasing the length of the chain further will only have marginal effects on the magnitude of the interaction and thus on the critical point of the system.

We used the relations obtained in Sec. 2.4 to apply our results for different ratios  $L/d$  to a wide range of lattices, shown in Fig. 4.13. The lower boundary for the tube spacing on the lattice is roughly  $d = 3$  in reduced units for a physical

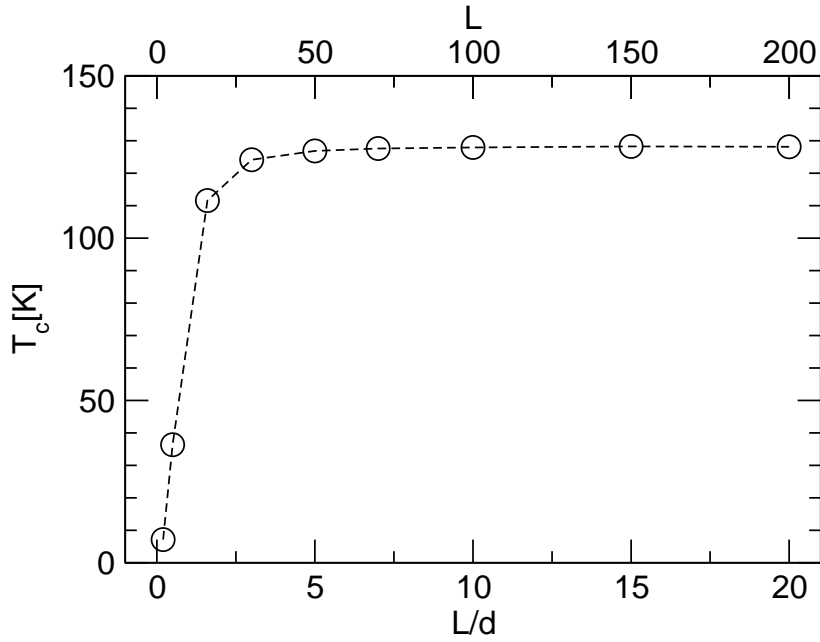


Figure 4.12: Critical temperature  $T_c$  of systems with a lattice spacing  $d = 10$ . The number of dipoles per chain is varied from 2 to 200. As expected, the obtained value for the critical point converges for large tube lengths.

system, lower values of  $d$  describe model properties rather than properties of membranes.

The isolines for the critical temperature illustrate the aforementioned behavior which can be seen in Fig. 4.14. For values of  $L/d \gtrsim 5$  the lines of constant  $T_c$  only depend weakly on the ratio  $L/d$  and the critical temperature of the system is determined by the absolute values of  $L$  and  $d$ .

This implies that the ratio  $L/d$  only has a marginal impact on the value of the critical temperatures for large membranes.

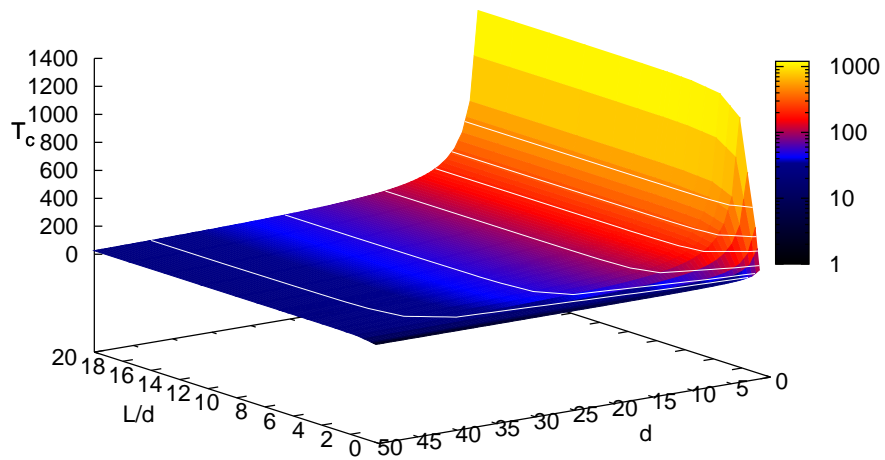


Figure 4.13: Critical temperatures  $T_c$ [K] as a function of tube length  $L$  and tube spacing  $d$ . For each constant ratio  $L/d$  lattices with  $d$  ranging from 1 to 50 were computed, intermediate values were interpolated. The white isolines characterize critical temperatures of 30, 50, 100, 200, 300 and 500 K.

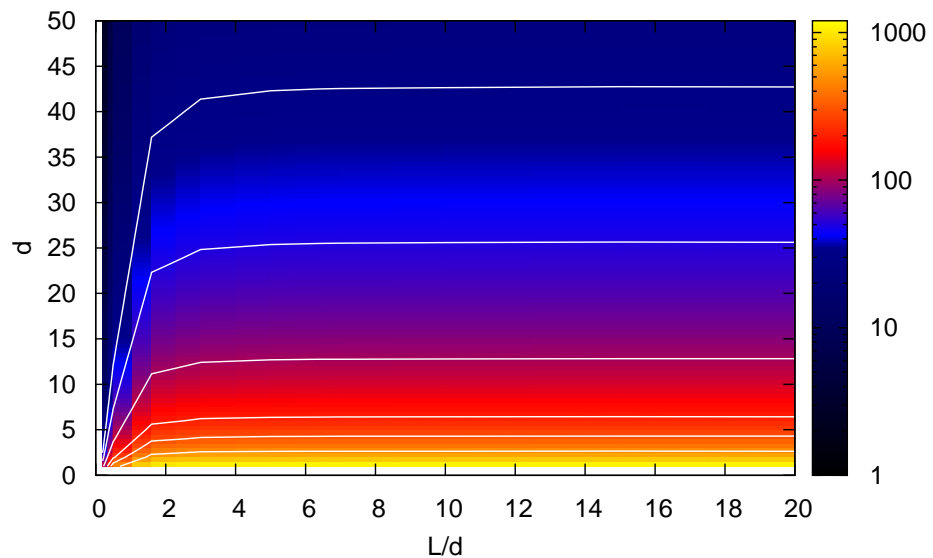


Figure 4.14: Top view onto Fig. 4.13, colors represent  $T_c$  [K] for a membrane of length  $L$  and lattice spacing  $d$ . Isolines are identical to Fig. 4.13.



## Chapter 5

# Final Remarks

We investigated the properties of a water filled membrane of carbon nanotubes using a dipole lattice model for the parallel water wires in the pores of the membrane. Since filling-emptying transitions in the pores and defect formation in the water chains were neglected for simplicity, we were able to reduce the problem to a two-dimensional spin lattice.

This spin model exhibits remarkable properties, most notably the corresponding states between lattices with an identical ratio between tube length and tube spacing. This property stems from the nature of the interaction in our model and is thus independent of the lattice geometry. Studying different lattice geometries with the aid of this property seems to be a promising undertaking, specifically on triangular lattices where the geometry leads to frustration in the system.

How do our results relate to “real world membranes”? Membranes realized in an experimental setting have large tube spacings [7], which lead to low critical temperatures for the lattice. Considering that the simplifications introduced to our model, such as exclusion of defect formation in the chains, neglecting possible screening effects and the placement of the tubes on a quadratic lattice, all lead to critical temperatures which are higher or equal to those obtained from systems without these simplifications, we conclude that antiferroelectric ordering at room temperature cannot be expected in membranes which can currently be realized in experiment.

In order to model the physical membrane more accurately, it will be necessary to study the interaction between the walls of the nanotubes and the water chains with a focus on screening effects between the water wires. If the screening can be approximated with sufficient accuracy by the introduction of a dielectric constant, our model can be easily modified to include such effects. However, if screening occurs in the system, this will further decrease the coupling of the water chains,

thus decreasing the critical temperature of the system further.

Our results indicate that membranes of experimentally feasible dimensions at room temperature are characterized well by previous studies of individual water chains in carbon nanopores [3, 13] due to the weak coupling between the water chains in the membrane. By measuring the dielectric response of a water filled membrane, the validity of this assumption can be evaluated in experiment.

# Bibliography

- [1] K. Koga, G. T. Gao, H. Tanaka, and X. C. Zeng. Formation of ordered ice nanotubes inside carbon nanotubes. *Nature*, 412:802–805, 2001.
- [2] G. Hummer, J. C. Rasaiah, and J. P. Noworyta. Water conduction through the hydrophobic channel of a carbon nanotube. *Nature*, 414(6860):188–190, Nov 2001.
- [3] Jürgen Köfinger, Gerhard Hummer, and Christoph Dellago. Macroscopically ordered water in nanopores. *Proceedings of the National Academy of Sciences*, 105(36):13218–13222, 2008.
- [4] Biswaroop Mukherjee, Prabal K. Maiti, Chandan Dasgupta, and Ajay K. Sood. Strongly anisotropic orientational relaxation of water molecules in narrow carbon nanotubes and nanorings. *ACS Nano*, 2(6):1189–1196, 2008.
- [5] Christoph Dellago, Mor M. Naor, and Gerhard Hummer. Proton transport through water-filled carbon nanotubes. *Phys. Rev. Lett.*, 90(10):105902, Mar 2003.
- [6] Jayendran C. Rasaiah, Shekhar Garde, and Gerhard Hummer. Water in nonpolar confinement: From nanotubes to proteins and beyond. *Annual Review of Physical Chemistry*, 59(1):713–740, 2008. PMID: 18092942.
- [7] Francesco Fornasiero, Hyung Gyu Park, Jason K. Holt, Michael Stadermann, Costas P. Grigoropoulos, Aleksandr Noy, and Olgica Bakajin. Ion exclusion by sub-2-nm carbon nanotube pores. *Proceedings of the National Academy of Sciences*, 105(45):17250–17255, 2008.
- [8] Ben Corry. Designing carbon nanotube membranes for efficient water desalination. *The Journal of Physical Chemistry B*, 112(5):1427–1434, 2008.
- [9] Klaus-Dieter Kreuer, Stephen J. Paddison, Eckhard Spohr, and Michael Schuster. Transport in proton conductors for fuel-cell applications: Sim-

- ulations, elementary reactions, and phenomenology. *Chemical Reviews*, 104(10):4637–4678, 2004.
- [10] Shigeo Maruyama, Erik Einarsson, Yoichi Murakami, and Tadao Edamura. Growth process of vertically aligned single-walled carbon nanotubes. *Chemical Physics Letters*, 403(4–6):320–323, 2005.
- [11] Kenji Hata, Don N. Futaba, Kohei Mizuno, Tatsunori Namai, Motoo Yumura, and Sumio Iijima. Water-assisted highly efficient synthesis of impurity-free single-walled carbon nanotubes. *Science*, 306:1362–1364, 2004.
- [12] Christoph Dellago and Mor M. Naor. Dipole moment of water molecules in narrow pores. *Computer Physics Communications*, 169(1-3):36–39, 2005. Proceedings of the Europhysics Conference on Computational Physics 2004.
- [13] Jürgen Köfinger, Gerhard Hummer, and Christoph Dellago. A one-dimensional dipole lattice model for water in narrow nanopores. *The Journal of Chemical Physics*, 130(15):154110, 2009.
- [14] Christoph Dellago and Gerhard Hummer. Kinetics and mechanism of proton transport across membrane nanopores. *Physical Review Letters*, 97(24):245901, 2006.
- [15] Erik Luijten and Henk W. J. Blöte. Classical critical behavior of spin models with long-range interactions. *Phys. Rev. B*, 56(14):8945–8958, Oct 1997.
- [16] Amrit Kalra, Shekhar Garde, and Gerhard Hummer. Osmotic water transport through carbon nanotube membranes. *Proceedings of the National Academy of Sciences*, 100(18):10175–10180, 2003.
- [17] Jason K. Holt, Hyung Gyu Park, Yinmin Wang, Michael Stadermann, Alexander B. Artyukhin, Costas P. Grigoropoulos, Aleksandr Noy, and Olga Bakajin. Fast Mass Transport Through Sub-2-Nanometer Carbon Nanotubes. *Science*, 312(5776):1034–1037, 2006.
- [18] Kerson Huang. *Statistical Mechanics*. Wiley, April 1987.
- [19] R. J. Baxter. *Exactly Solved Models in Statistical Mechanics*. Academic Press, London, 1982.
- [20] Lars Onsager. Crystal statistics. i. a two-dimensional model with an order-disorder transition. *Phys. Rev.*, 65(3-4):117–149, Feb 1944.

- [21] David Chandler. *Introduction to Modern Statistical Mechanics*. Oxford University Press, 1. edition, 1987.
- [22] William Humphrey, Andrew Dalke, and Klaus Schulten. VMD – Visual Molecular Dynamics. *Journal of Molecular Graphics*, 14:33–38, 1996.
- [23] Franz Schwabl. *Statistical Mechanics*. Springer, 2006.
- [24] Kurt Binder. Theory of first-order phase transitions. *Rep. Prog. Phys.*, 50:783–859, 1987.
- [25] Daan Frenkel and Berend Smit. *Understanding Molecular Simulation*. Academic Press, New York, 2002.
- [26] M. Metropolis, A. W. Rosenbluth, M. N. Rosenbluth, A. N. Teller, and E. Teller. Equation of state calculations by fast computing machines. *J. Chem. Phys.*, 21:1087, 1953.
- [27] Fugao Wang and D. P. Landau. Determining the density of states for classical statistical models: A random walk algorithm to produce a flat histogram. *Phys. Rev. E*, 64(5):056101, Oct 2001.
- [28] F. Calvo. Sampling along reaction coordinates with the wang-landau method. *Mol. Phys.*, 100(21):3421, 2002.
- [29] Robert H. Swendsen and Jian-Sheng Wang. Nonuniversal critical dynamics in monte carlo simulations. *Phys. Rev. Lett.*, 58(2):86–88, Jan 1987.
- [30] Alan M. Ferrenberg and Robert H. Swendsen. New monte carlo technique for studying phase transitions. *Phys. Rev. Lett.*, 61(23):2635–2638, Dec 1988.
- [31] Athanassios Panagiotopoulos. Monte carlo methods for phase equilibria of fluids. *Journal of Physics: Condensed Matter*, 12(3):R25–52, 2000.
- [32] David Landau and Kurt Binder. *A Guide to Monte Carlo Simulations in Statistical Physics*. Cambridge University Press, New York, NY, USA, 2000.
- [33] Nigel B. Wilding. Critical-point and coexistence-curve properties of the lennard-jones fluid: A finite-size scaling study. *Phys. Rev. E*, 52(1):602–611, Jul 1995.
- [34] Mike P. Allen and D. J. Tildesley. *Computer Simulation of Liquids*. Clarendon Press, Oxford, 1991.

- 
- [35] A. Grzybowski, E. Gwóźdź, and A. Bródka. Ewald summation of electrostatic interactions in molecular dynamics of a three-dimensional system with periodicity in two directions. *Phys. Rev. B*, 61(10):6706–6712, Mar 2000.
- [36] A. Bródka. Ewald summation method with electrostatic layer correction for interactions of point dipoles in slab geometry. *Chemical Physics Letters*, 400(1-3):62–67, 2004.
- [37] Michael E. Fisher. The renormalization group in the theory of critical behavior. *Rev. Mod. Phys.*, 46(4):597–616, Oct 1974.
- [38] Michael E. Fisher. The theory of equilibrium critical phenomena. *Reports on Progress in Physics*, 30(2):615, 1967.
- [39] R Hilfer and N B Wilding. Are critical finite-size scaling functions calculable from knowledge of an appropriate critical exponent? *Journal of Physics A: Mathematical and General*, 28(10):L281–L286, 1995.
- [40] Jürgen Köfinger, Nigel B. Wilding, and Gerhard Kahl. Phase behavior of a symmetrical binary fluid mixture. *J. Chem. Phys.*, 125(23), Dec. 21 2006.
- [41] Jürgen Köfinger, G. Kahl, and N. B. Wilding. Phase behaviour of a symmetrical binary mixture in a field. *Europhys. Lett.*, 75(2):234, Jul 2006.
- [42] Kurt Binder. Finite size scaling analysis of ising model block distribution functions. *Zeitschrift für Physik B Condensed Matter*, 43(2):119–140, 1981.